2004

Defect detection in correlated noise

Nawanat Eua-Anant
Iowa State University

Defect detection in correlated noise

by

Nawanat Eua-Anant

A thesis submitted to the graduate faculty

in partial fulfillment of the requirements for the degree of

MASTER OF SCIENCE

Major: Electrical Engineering

Program of Study Committee:
Aleksandar Dogandžić, Major Professor
Joseph N. Gray
Zhengdao Wang

Iowa State University

Ames, Iowa

2004

Graduate College
Iowa State University

This is to certify that the master's thesis of

Nawanat Eua-Anant

has met the thesis requirements of Iowa State University

Signature redacted for privacy

Major Professor

Signature redacted for privacy

For the Major Program

DEDICATION

I would like to dedicate this thesis to my mother and father, Yaowalak and Subhon Eua-Anant in appreciation for their unconditional love, support, and encouragement throughout my graduate study.

TABLE OF CONTENTS

LIST OF TABLES

LIST OF FIGURES

ABSTRACT

Nondestructive evaluation (NDE) has been extensively used for investigating the integrity of materials and characterizing cracks or defects. We present methods for detecting NDE defect signals in correlated noise having unknown covariance. The proposed detectors are derived using the statistical theory of generalized likelihood ratio (GLR) tests and multivariate analysis of variance (MANOVA). We consider both real and complex data models for data sets obtained from multiple experiments. To allow accurate estimation of the noise covariance, we incorporate secondary data containing only noise into the detector design. Probability distributions of the GLR test statistics are derived under the null hypothesis, i.e. assuming that the signal is absent, and used for the detector design. We also develop a numerical method for computing the exact decision threshold that guarantees a specified probability of false alarms. We apply the proposed methods to simulated and experimental data and demonstrate their superior performance compared with the detectors that neglect noise correlation.

CHAPTER 1. INTRODUCTION

In the recent years, nondestructive evaluation (NDE) has been extensively used as a major methodology for investigating the integrity of materials and characterizing cracks or defects. It has been applied to several applications in industrial inspections such as crack detection in airplane wheels and investigation of steam generator tubes in nuclear power and chemical plants. Undesirable cracks or defects may originate in a material during manufacturing, or from fatigue or stress corrosion during service. The proper inspection and monitoring of the presence of defects are necessary and critical in order to assure the quality of products during manufacturing processes and also the reliability of systems which consequently can prevent accidents that can cost human lives. It also helps predicting the remaining life of the structural components. A variety of methods for NDE have been developed in response to the raising demands of industries such as eddy current [1], ultrasonic [2], and X-ray radiography [3].

Eddy-current inspection is a testing technique using the principle of electromagnetism as the basis for conducting examinations. Eddy current is generated by electromagnetic induction when alternating current is applied to a conductor such as copper wire. For defect detection, generally, an eddy-current probe consists of two sets of coils, the excitation or primary and the pick-up or secondary, arranged in a transformer fashion, see Figure 1.1. When the alternating current is applied to the excitation coil, it creates a magnetic field around the coil and induces eddy currents in the examined material. The pick-up coil acting as a detector will determine the change of impedance and phase corresponding to the change of conduction in the material. The concept of this probe provides an enhanced signal-to-noise ratio (SNR) for detection and significant advantage especially in the case when deep penetration is needed such as internal

defect inspection.

In ultrasonic inspection, high frequency sound energy is used to conduct examinations. An ultrasonic probe generally consists of the pulser/receiver, transducer, and measuring units. The pulser generates and sends a high voltage electrical pulse into the transducer. The high voltage energy is transformed into ultrasonic signals by the transducer and transmitted into an examined object in a wave form. The propagated waves are reflected back to the receiver as echoes when they reach the boundary of discontinuities such as the edge of the material, cracks, or defects. The reflected signals are reconverted into electrical signals by the transducer and then measured by the measuring units. This technique is generally used for detecting and classifying cracks or defects and also determining the size, orientation, and position of the reflectors. Figure 1.2 demonstrates how the ultrasonic signal is transmitted into the material and responds to the boundary of the material and crack. The strength of the received signal is plotted against the signal travel time.

Another common testing technique for NDE is X-ray radiography. This technique uses the principle of electromagnetic radiation. By this principle, a stream of electrons is energized and accelerated into a high velocity. Energy in the form of photons (or X-ray in this case) is emitted when the charged particles (electrons) are deaccelerated. This resulting X-ray beam is widely used to produce radiographs of materials and objects to locate internal cracks and other defects. The detectors can be films or a sensor array of light-sensitive photocells called Charge-Coupled Device (CCD), see Figure 1.3.

In the measurement processes of the methods above, undesirable noise is caused by several reasons such as the imperfection of measuring sensors, the nature of medium (e.g. grain noise), and interference from the surrounding environment, etc. In general, noise is modeled as random variables and its behavior is described by statistical distributions. By applying the Central Limit Theorem (CLT) [4, Ch. 5.5], we may use a normal or Gaussian distribution for noise models. The problem of interest is how to determine and account for noise correlation between measurement locations. In the NDE applications, the noise correlation is typically caused by

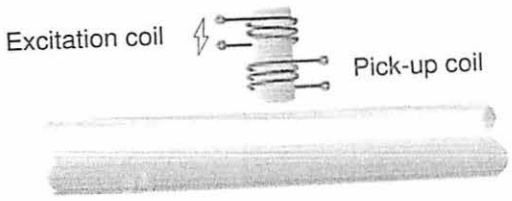

Figure 1.1 Eddy-current testing.

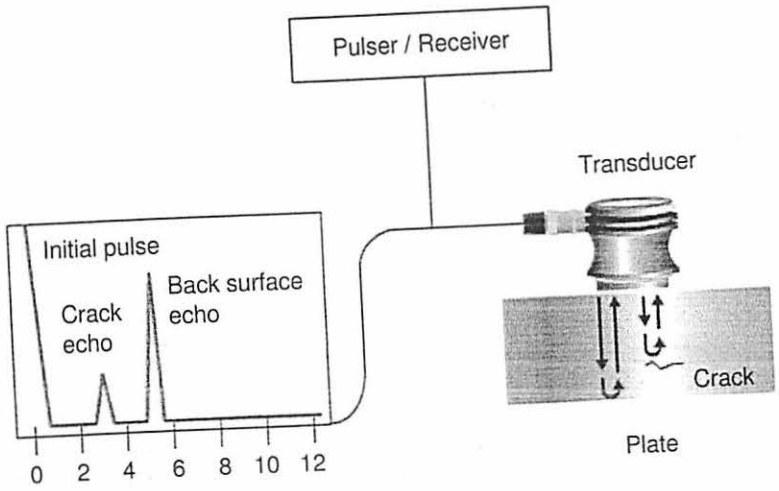

Figure 1.2 Ultrasonic testing.

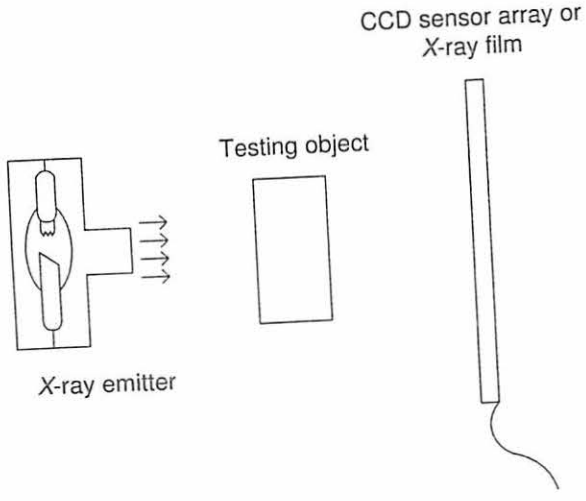

Figure 1.3 X-ray radiography.

- backscattered grain in ultrasonic NDE systems [5]and
- random liftoff variations in eddy-current systems [1].

Accounting for noise correlation in material inspection can significantly improve defect detection performance. This thesis primarily focuses on defect detection using statistical analysis. We introduce methods for detecting defects in two-dimensional images with correlated noise. The noise is assumed to be correlated between rows of data matrices having unknown covariance. The proposed detectors are derived using the statistical theory of generalized likelihood ratio (GLR) tests and multivariate analysis of variance (MANOVA) (see [6] for a tutorial presentation of MANOVA and [7, Ch. 6.4.2] for the definition of the GLR test). We consider real and complex data models and single- and multiple-trial measurement scenarios. For each data matrix under test, we assume that a noise-only matrix is available and utilize both the data and noise-only matrices to estimate the noise covariance. To decide if a defect is present, the GLR test statistic is compared with a threshold. We derive exact and approximate probability distributions of the GLR test statistics under the null hypothesis (signal absent) and use them to find the threshold that guarantees a specified probability of false alarms.

The rest of this thesis is organized as follows. In Chapter 2, we first introduce signal and noise models under single- and multiple-trial scenarios. We then present the GLR detectors for real and complex data models. Furthermore, we demonstrate the derivation of the exact distribution used to determine a decision threshold for a specified probability of false alarms. In Chapter 3, the proposed methods have been applied to simulated eddy-current, experimental ultrasonic, and experimental X-ray data, and compared with energy detectors that do not account for noise correlation. Finally in Chapter 4, we conclude the thesis by outlining suggestions for future work and providing an example algorithm that can improve the detection and eliminate false alarms.

CHAPTER 2. METHODS AND PROCEDURES

2.1 Introduction

The objective of this chapter is to study and discuss the definition of data models, the derivation of the generalize likelihood ratio (GLR) tests, and a proposed method used to determine the exact probability distributions and decision rules for the tests. Moreover, we compare the accuracy of the proposed algorithm to traditional approximate methods.

2.2 Signal and Noise Models

In this section, we first present signal and noise models for a single experiment (trial) and then extend them to the multiple-trial scenario.

2.2.1 Single Trial

We consider the problem of detecting the presence of a defect signal in an $m \times d$ data matrix under test $\boldsymbol{Y}_{\mathrm{T}}$. A noise-only data matrix $\boldsymbol{Z}$ of size $m \times (N-d)$ is also assumed to be available. Figure 2.1 illustrates the arrangement of matrices $\boldsymbol{Y}_{\mathrm{T}}$ and $\boldsymbol{Z}$. If we do not have *any* additional information about the nature of the defect signal, we can choose a *nonparametric* model for the signal mean:

$$\mathrm{E}\left[\boldsymbol{Y}_{\mathrm{T}}\right] = \boldsymbol{X}, \tag{2.1}$$

where $\boldsymbol{X}$ is a matrix of unknown parameters and E[·] denotes expectation. For real measurements, we further model the columns of $\boldsymbol{Y}_{\mathrm{T}}$ as independent Gaussian vectors with an *unknown*

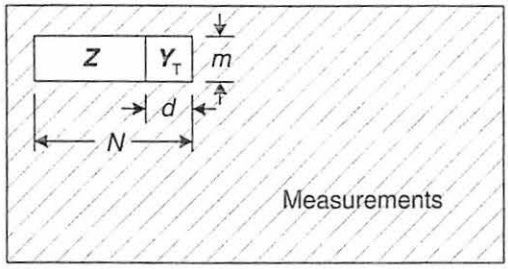

Figure 2.1 Matrix under test $\boldsymbol{Y}_{\mathrm{T}}$ and noise-only matrix $\boldsymbol{Z}$.

$m \times m$ positive definite covariance matrix $\boldsymbol{\Sigma}$. The columns of the noise-only matrix $\boldsymbol{Z}$ are assumed to be independent zero-mean Gaussian vectors with covariance $\boldsymbol{\Sigma}$. Similarly, for complex measurements, we assume that (2.1) holds, the columns of $\boldsymbol{Y}_{\mathrm{T}}$ are independent circularly symmetric complex Gaussian vectors with an unknown positive definite covariance $\boldsymbol{\Sigma}$, and the columns of $\boldsymbol{Z}$ are independent circularly symmetric zero-mean complex Gaussian vectors with covariance $\boldsymbol{\Sigma}$.

2.2.2 Multiple Trials

In some NDE applications, the experiment in which the measurements are collected is repeated K times to improve the signal-to-noise ratio (SNR). Denote the data matrix under test in the kth trial by $\boldsymbol{Y}_{\mathrm{T},k}$ and the corresponding noise-only matrix by $\boldsymbol{Z}_k$, where $k = 1, 2, \ldots, K$. We assume that the defect signal is the same in all trials (independent of k), i.e.

$$\mathrm{E}\left[\boldsymbol{Y}_{\mathrm{T},k}\right] = \boldsymbol{X}, \quad k = 1, 2, \ldots, K \tag{2.2}$$

and that the noise is independent between trials and has the same covariance $\boldsymbol{\Sigma}$ (independent of k) in each trial. We also assume that

$$NK \geq m + d,$$

which is needed to ensure that we can estimate Σ. This condition follows from [8, App. C] and [9, App. B], see also [6, eq. (4)].

2.3 Generalized Likelihood Ratio Tests

We develop the GLR tests for detecting defects based on the above measurement model under both real and complex data scenarios. The GLR tests are useful in a case when signal and noise parameters are unknown, see [7].

2.3.1 Hypothesis Testing

In order to detect the presence of a defect signal, we test the null hypothesis $\mathcal{H}_0 : X = 0$ (no defect present) versus the alternative $\mathcal{H}_1 : X \neq 0$ (defect present). We wish to design a test which maximizes the probability of detection (P_{D}) and satisfies the probability of false alarms (P_{FA}). Figure 2.2 shows the probability density functions (PDF) of a test statistic under $\mathcal{H}_0$ and $\mathcal{H}_1$ and the relation between P_{D} and P_{FA} where in this case, $P_{\mathrm{FA}} = P(\text{test statistic} > \tau; \mathcal{H}_0)$ and $P_{\mathrm{D}} = P(\text{test statistic} > \tau; \mathcal{H}_1)$. If such an ideal test exists for all possible parameter values, it is called a uniformly most powerful (UMP) test. Generally, UMP tests do not exist for composite hypothesis testing problems. A simple suboptimal solution with good asymptotic properties is the generalized likelihood ratio test. To compute the GLR test:

$$\mathrm{GLR} = \frac{\text{maximum likelihood under } \mathcal{H}_1}{\text{maximum likelihood under } \mathcal{H}_0}$$

or any monotonic function of the right side and compare GLR with a threshold τ. Note that for the test statistic above, we need to specify a constraint for P_{FA}; otherwise we could always declare the presence of a defect and have $P_{\mathrm{D}} = 1$ but we also have $P_{\mathrm{FA}} = 1$.

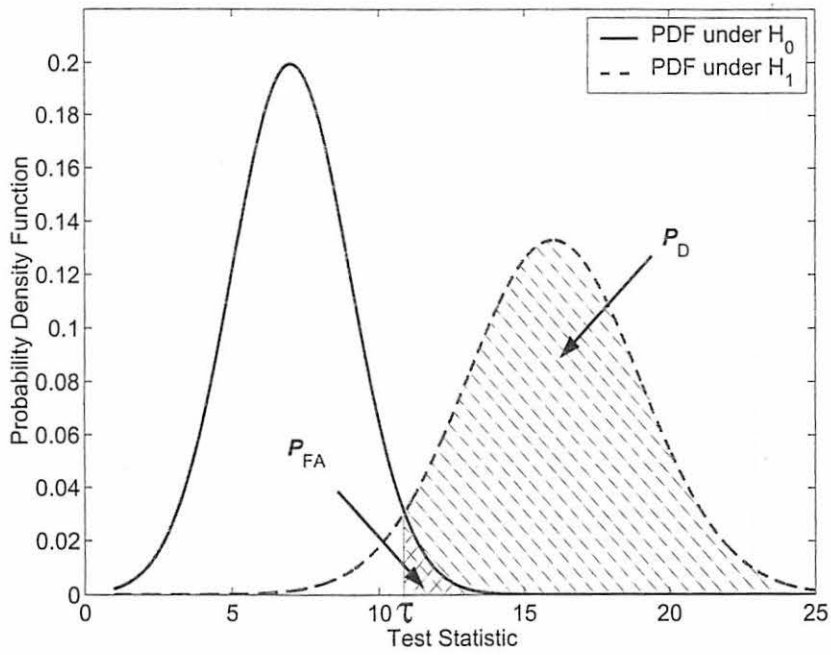

Figure 2.2 P_{FA} and P_{D}.

2.3.2 GLR Test for Real Data

Assuming real measurements, to detect the defect signal, we utilize both the data matrices under test $\boldsymbol{Y}_{\mathrm{T},k}$ and noise matrices $\boldsymbol{Z}_k$. The GLR test computes the ratio of likelihood functions under the two hypotheses, with unknown parameters ($\boldsymbol{X}$ and $\boldsymbol{\Sigma}$ under $\mathcal{H}_0$ and $\boldsymbol{\Sigma}$ under $\mathcal{H}_1$) replaced by their maximum likelihood (ML) estimates. First, define the sufficient statistics for estimating $\boldsymbol{X}$ and $\boldsymbol{\Sigma}$:

$$\overline{\boldsymbol{Y}}_{\mathrm{T}} = \frac{1}{K}\sum_{k=1}^{K}\boldsymbol{Y}_{\mathrm{T},k}, \tag{2.3a}$$

$$\widehat{\boldsymbol{R}} = \frac{1}{NK}\sum_{k=1}^{K}(\boldsymbol{Y}_{\mathrm{T},k}\boldsymbol{Y}_{\mathrm{T},k}{}^{T} + \boldsymbol{Z}_k\boldsymbol{Z}_k{}^{T}), \tag{2.3b}$$

where "^{T}" denotes a transpose. The GLR test compares

$$\text{GLR} = \frac{|\widehat{\boldsymbol{R}}|}{|\widehat{\boldsymbol{R}} - (1/N) \cdot \overline{\boldsymbol{Y}}_{\text{T}} \overline{\boldsymbol{Y}}_{\text{T}}^{T}|} = \frac{1}{|\boldsymbol{I}_d - (1/N) \cdot \overline{\boldsymbol{Y}}_{\text{T}}^{T} \widehat{\boldsymbol{R}}^{-1} \overline{\boldsymbol{Y}}_{\text{T}}|} \tag{2.4}$$

with a threshold, where the presence of a defect is declared if GLR is greater than a threshold. Here $|\cdot|$ denotes the determinant. The above test can be derived using the results of [8] and [9], where estimation and detection algorithms were developed for a more general measurement model and applied to the analysis of evoked responses using electroencephalography/magnetoencephalography (EEG/MEG) arrays. Interestingly, in the scalar case and if the zero-mean data is not available (i.e. $m = d = N = 1$) and after the monotonic transformation $\sqrt{\text{GLR} - 1}$, the GLR expression (2.4) reduces to the familiar t-test: $\overline{y}/\sqrt{s^2}$, where $\overline{y} = \sum_{k=1}^{K} y_k/K$ and $s^2 = \sum_{k=1}^{K}(y_k - \overline{y})^2/K$.

2.3.3 GLR Test for Complex Data

For complex measurements, the sufficient and GLR test statistics follow by replacing "^{T}" in (2.3) and (2.4) with "^{H}", respectively, where "^{H}" denotes the Hermitian (conjugate) transpose. Hence, the sufficient statistics and GLR test for a complex data case can be expressed as follows:

$$\overline{\boldsymbol{Y}}_{\text{T}} = \frac{1}{K} \sum_{k=1}^{K} \boldsymbol{Y}_{\text{T},k}, \tag{2.5a}$$

$$\widehat{\boldsymbol{R}} = \frac{1}{NK} \sum_{k=1}^{K} (\boldsymbol{Y}_{\text{T},k} \boldsymbol{Y}_{\text{T},k}^{H} + \boldsymbol{Z}_k \boldsymbol{Z}_k^{H}), \tag{2.5b}$$

$$\text{GLR} = \frac{|\widehat{\boldsymbol{R}}|}{|\widehat{\boldsymbol{R}} - (1/N) \cdot \overline{\boldsymbol{Y}}_{\text{T}} \overline{\boldsymbol{Y}}_{\text{T}}^{H}|} = \frac{1}{|\boldsymbol{I}_d - (1/N) \cdot \overline{\boldsymbol{Y}}_{\text{T}}^{H} \widehat{\boldsymbol{R}}^{-1} \overline{\boldsymbol{Y}}_{\text{T}}|}. \tag{2.5c}$$

2.4 GLR Distribution Under Null Hypothesis

2.4.1 GLR Distribution for Real Data

For real measurements and under $\mathcal{H}_0$, the probability distribution of $1/\mathrm{GLR}$ is (see Appendix A)

$$\frac{1}{\mathrm{GLR}} \sim \lambda(m, NK-d, d).$$

where λ denotes the Wilks' lambda distribution. The above Wilks' lambda distribution is the distribution of the product of m independent beta random variables with parameters $\left(\frac{1}{2}(NK-d-i+1), \frac{1}{2}d\right)$, $i = 1, 2, \ldots, m$. Since Wilks' lambda distribution does not depend on the unknown parameters ($\boldsymbol{\Sigma}$ in this case), we can compute a threshold τ that maintains a constant probability of false alarms. Such a detector is referred to as a *constant false-alarm rate* (CFAR) detector, see e.g. [7]. For large $NK-d$ (i.e. $NK-d \gg \max\{m,d\}$), the following approximation can be used to compute τ for a specified false-alarm probability (see e.g. [10, Cor. 4.2.1]):

$$P_{\mathrm{FA}} = P\{[NK - \tfrac{1}{2}(d+m+1)] \cdot \ln \mathrm{GLR} \geq \tau\} \approx P\{\chi^2_{md} \geq \tau\} \tag{2.6}$$

or

$$\begin{aligned} P_{\mathrm{FA}} &= P\{[NK - \tfrac{1}{2}(d+m+1)] \cdot \ln \mathrm{GLR} \geq \tau\} \\ &\approx P\{\chi^2_{md} \geq \tau\} + \frac{md(m^2+d-5)}{48(NK-d)^2} \cdot [P\{\chi^2_{md} \geq \tau\} + P\{\chi^2_{md} \geq \tau\}] \end{aligned} \tag{2.7}$$

for more accuracy, where χ^2_{md} denotes a χ^2 random variable with md degrees of freedom. However, the above approximate distributions are not accurate when the number of observations is small, for an example, see Figure 2.3. Figure 2.3 demonstrates a scenario in which the approximate distributions in (2.6) and (2.7) do not match the result obtained by Monte Carlo simulation [11, 12]. In this example, we simulate a situation that the test has a small number of observations by choosing $N = 15, K = 1, m = 5$, and $d = 5$. The density using Monte Carlo

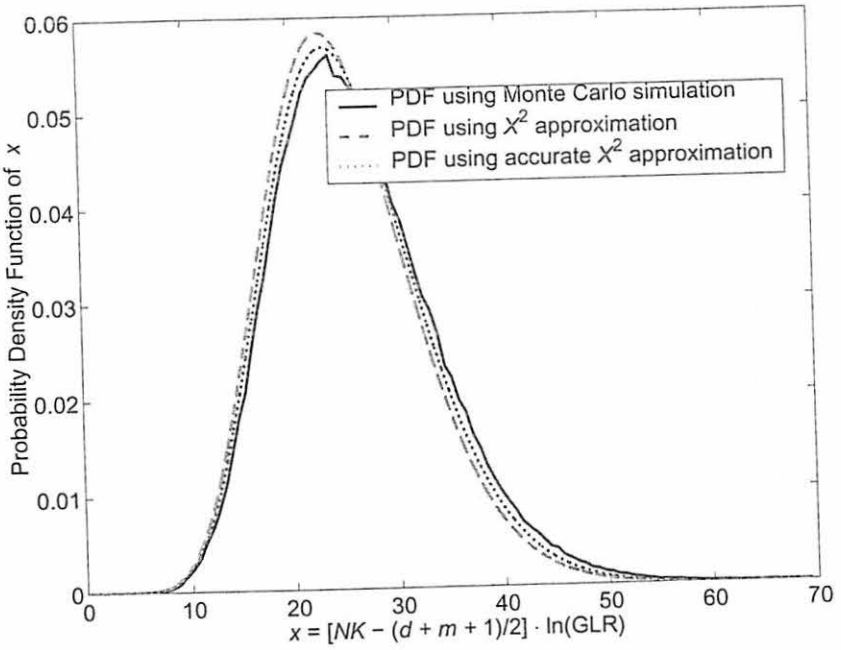

Figure 2.3 Approximate PDFs for a real data scenario when $N = 15$, $K = 1$, $m = 5$, and $d = 5$.

simulation was calculated by averaging 300,000 realizations over 100 bins.

To overcome this problem, we develop an algorithm for computing the exact distribution of the GLR test, see Appendix C. For real measurements, the PDF of the GLR test can be computed using the following infinite series:

$$f(\lambda) = \Big[\prod_{j=1}^{m} \frac{\Gamma(\frac{NK-m+j}{2})}{\Gamma(\frac{NK-m-d+j}{2})}\Big] \lambda^{\mu-1} \sum_{r=0}^{\infty} \frac{l_r}{\Gamma(r+md/2)} (-\ln \lambda)^{r+\frac{md}{2}-1} \tag{2.8}$$

and the GLR threshold for a specified P_{FA} can be determined by solving the following equation:

$$P_{\text{FA}} = P(\text{GLR} > \tau) = 1 - \Big[\prod_{j=1}^{m} \frac{\Gamma(\frac{NK-m+j}{2})}{\Gamma(\frac{NK-m-d+j}{2})}\Big] \sum_{r=0}^{\infty} \frac{l_r}{\mu^{(r+md/2)}} \Gamma_{\text{inc}}\Big(\mu \ln \tau,\ r + \frac{md}{2}\Big) \tag{2.9}$$

where $\lambda = 1/\text{GLR}$ and $\Gamma_{\text{inc}}(x, a)$ is the incomplete gamma function at value x with parameter a. Here μ is a constant chosen to satisfy $0 \le \mu < (NK-m-d+1)/2$; $l_0 = 1$, $l_r = \sum_{k=1}^{r} k\, q_k\, l_{r-k}$,

and

$$q_k = (-1)^{k+1}[k(k+1)]^{-1}\Big\{\sum_{j=1}^{m} B_{k+1}\Big(\frac{NK-m-d+j}{2}-\mu\Big) - \sum_{j=1}^{m} B_{k+1}\Big(\frac{NK-m+j}{2}-\mu\Big)\Big\},\ k=1,2,\ldots$$

and $B_r(\cdot)$ denotes the Bernoulli polynomial of degree r. (Since P_{FA} is a monotonic function, we may apply a bisection method [13, Ch. 8.1] to solve the above equation.) Using the same set of parameters in the previous example, Figures 2.4 and 2.5 show the superior result compared to the traditional approximations. We now compare the PDFs using the above methods in the case when the simple form of the PDF is known, i.e. when $m = 1$, the GLR test has the same distribution as a single beta random variable. In this case, we choose $N = 8, K = 1, m = 1$, and $d = 4$. In Figures 2.6 and 2.7, the PDF using the proposed method provides a superior result which exactly matches the theoretical PDF whereas the approximate methods do not. Table 2.1 demonstrates the comparison of the GLR thresholds obtained from various methods in the case when the simple form of the PDF is known ($m = 1$). Obviously, the proposed method outperforms the traditional approximations. However, when the number of observations increases, the thresholds obtained from the approximate methods asymptotically approach the thresholds obtained from the theoretical PDF.

2.4.2 GLR Distribution for Complex Data

For complex measurements and under $\mathcal{H}_0$, 1/GLR follows the complex Wilks' lambda distribution, see e.g. [14], and it can be represented by the product of m independent beta random variables with parameters $\big(NK-d-i+1, d\big)$, $i = 1, 2, \ldots, m$. As in the real case, the resulting detector is CFAR. For large $NK-d$, the traditional approximation for computing

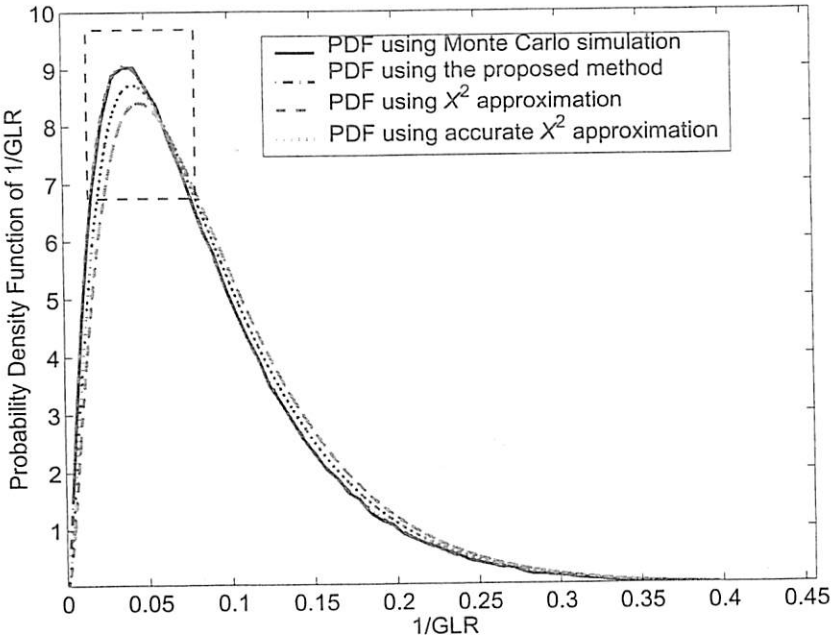

Figure 2.4 Comparison of PDFs for a real data scenario when $N = 15$, $K = 1$, $m = 5$, and $d = 5$.

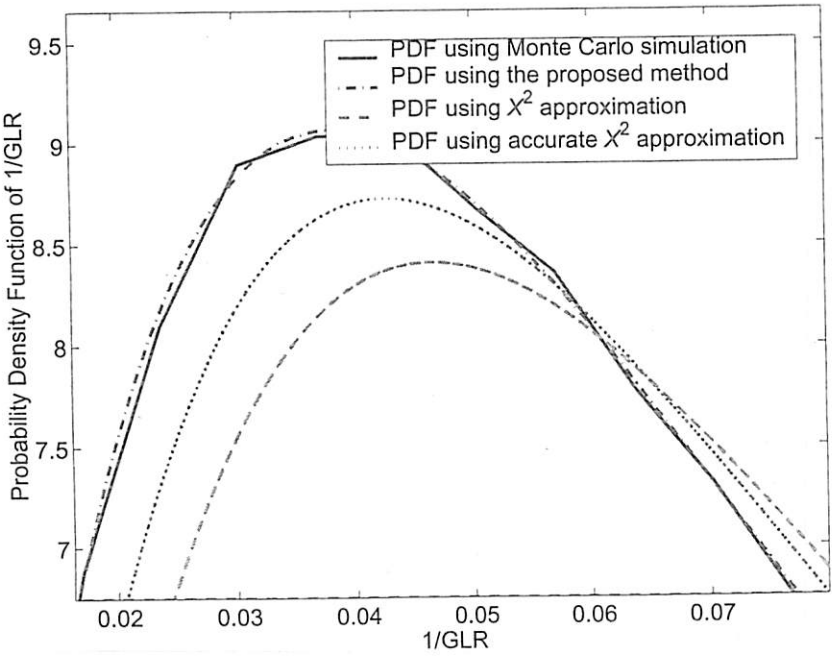

Figure 2.5 Comparison of PDFs in the dash area of Figure 2.4.

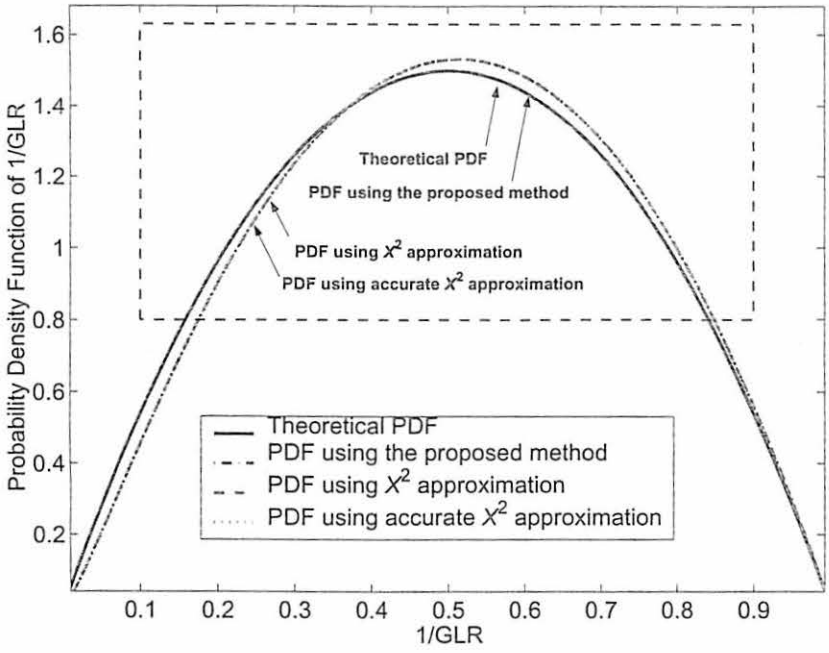

Figure 2.6 Comparison of PDFs for a real data scenario when $N = 8$, $K = 1$, $m = 1$, and $d = 4$.

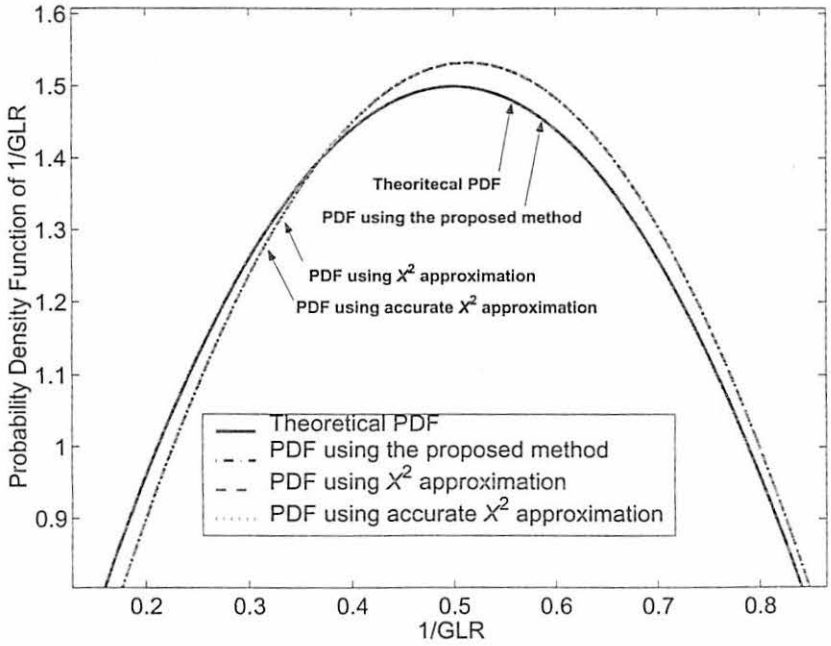

Figure 2.7 Comparison of PDFs in the dash area of Figure 2.6.

Table 2.1 Comparison of thresholds obtained from various methods under a real data scenario. Here, 1, 2, 3, and 4 denote thresholds obtained from the theoretical PDF, proposed method, χ^2 approximation, and accurate χ^2 approximation, respectively.

m	$NK-d$	d	P_{FA} (%)	Thresholds			
				1	2	3	4
1	4	4	2	11.8994	11.8994	10.3147	10.3147
1	4	4	1	16.9770	16.9770	14.2300	14.2300
1	4	4	0.5	24.1545	24.1545	19.5300	19.5300
1	6	4	2	5.5729	5.5729	5.2954	5.2954
1	6	4	1	7.0988	7.0988	6.6637	7.0986
1	6	4	0.5	9.0183	9.0183	8.3547	8.3547
1	16	4	2	1.9934	1.9934	1.9864	1.9864
1	16	4	1	2.1931	2.1931	2.1836	2.1836
1	16	4	0.5	2.4094	2.4094	2.3967	2.3967

the threshold τ for a specified false-alarm probability is as follows:

$$P_{\text{FA}} = P\{(2NK - d - m - 1) \cdot \ln \text{GLR} \geq \tau\} \approx P\{\chi^2_{2md} \geq \tau\} \tag{2.10}$$

By applying the same method as in the real case, the exact PDF of the GLR test for the complex case can be represented by the following infinite series:

$$f(\lambda) = \Big[\prod_{j=1}^{m} \frac{\Gamma(NK-m+j)}{\Gamma(NK-m-d+j)}\Big] \lambda^{\mu-1} \sum_{r=0}^{\infty} \frac{l_r}{\Gamma(r+md)} (-\ln \lambda)^{r+md-1} \tag{2.11}$$

and the GLR threshold for a specified P_{FA} can be determined by solving the following equation:

$$P_{\text{FA}} = P(\text{GLR} > \tau) = 1 - \Big[\prod_{j=1}^{m} \frac{\Gamma(NK-m+j)}{\Gamma(NK-m+j)}\Big] \sum_{r=0}^{\infty} \frac{l_r}{\mu^{(r+md)}} \Gamma_{\text{inc}}(\mu \log \tau,\ r+md) \tag{2.12}$$

where μ is a constant chosen to satisfy $0 \leq \mu < (NK-m-d+1)$; $l_0 = 1$, $l_r = \sum_{k=1}^{r} k q_k l_{r-k}$, and

$$q_k = (-1)^{k+1}[k(k+1)]^{-1}\Big\{ \sum_{j=1}^{m} B_{k+1}(NK-m-d+j-\mu) - \sum_{j=1}^{m} B_{k+1}(NK-m+j-\mu)\Big\},\ k = 1, 2, \ldots.$$

Figures 2.8 and 2.9 shows the comparison of PDFs using Monte Carlo simulation and the methods above when $N = 20, K = 1, m = 5$, and $d = 5$. Figure 2.10 shows the comparison of PDFs when the theoretical PDF is known. Here, $N = 8, K = 1, m = 1$, and $d = 4$. Table 2.2 demonstrates the comparison of the GLR thresholds obtained from various methods in the case when the simple form of the PDF is known. As in the real case, the proposed method outperforms the traditional approximation.

Table 2.2 Comparison of thresholds obtained from various methods under a complex data scenario. Here, 1, 2, and 3 denote thresholds obtained from the theoretical PDF, proposed method, and χ^2 approximation, respectively.

m	$NK-d$	d	P_{FA} (%)	**Thresholds**		
				1	**2**	**3**
1	4	4	2	5.7899	5.7899	6.1521
1	4	4	1	7.0288	7.0288	7.4559
1	4	4	0.5	8.4959	8.4958	8.9842
1	6	4	2	3.4932	3.4932	3.6609
1	6	4	1	3.9995	3.9995	4.1996
1	6	4	0.5	4.5633	4.5633	4.7979
1	16	4	2	1.6855	1.6855	1.7063
1	16	4	1	1.7816	1.7816	1.8055
1	16	4	0.5	1.8802	1.8802	1.9073

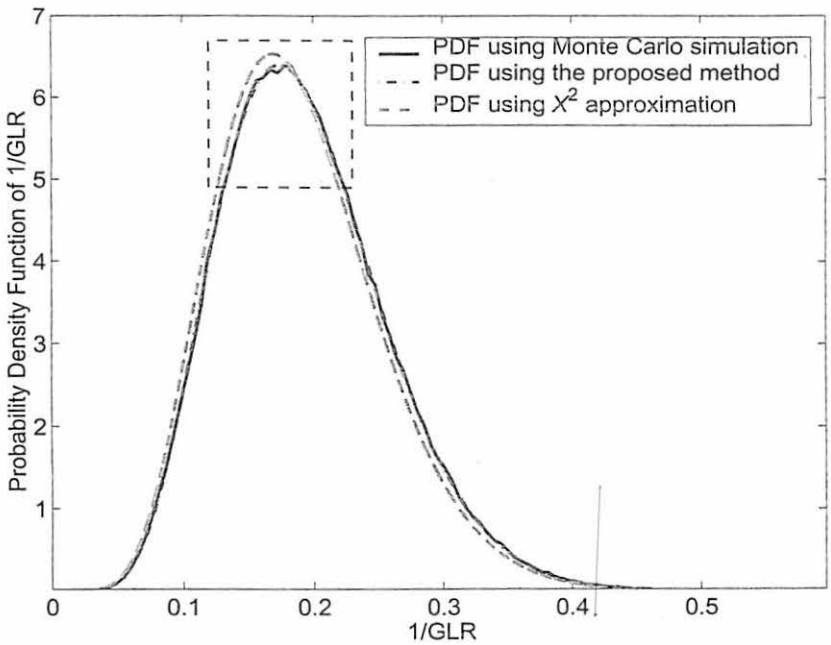

Figure 2.8 Comparison of PDFs for a complex data scenario when $N = 20$, $K = 1$, $m = 5$, and $d = 5$.

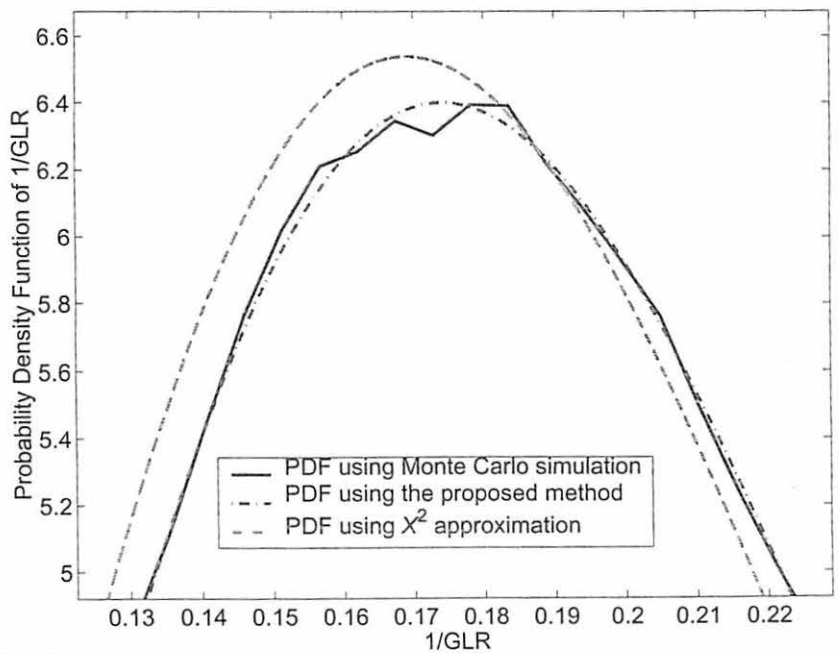

Figure 2.9 Comparison of PDFs in the dash area of Figure 2.8.

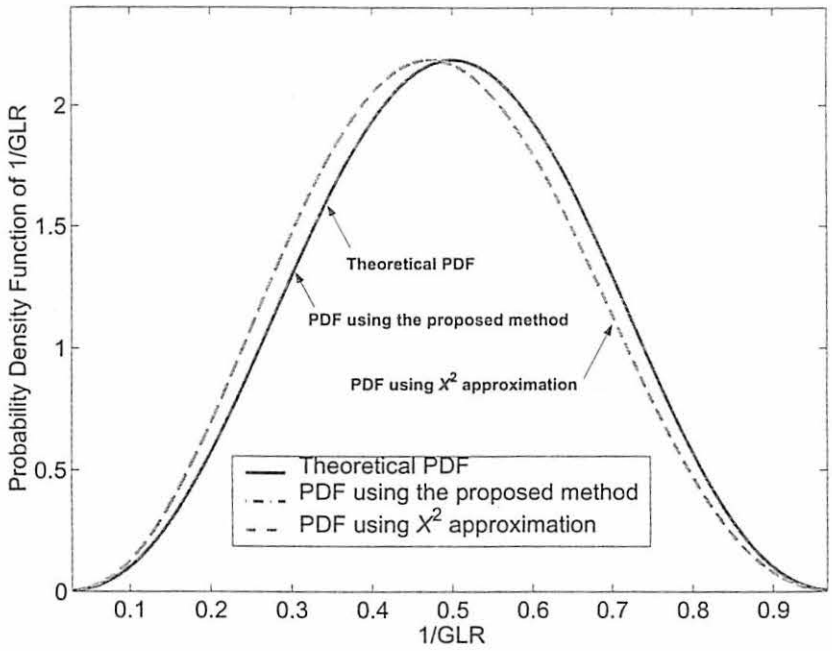

Figure 2.10 Comparison of PDFs for a complex data scenario when $N = 8$, $K = 1$, $m = 1$, and $d = 4$.

2.5 Mean-Data Energy Detector

In all numerical examples, we compare the proposed method with the CFAR energy detector (ED) for the mean data $\overline{\boldsymbol{Y}}_{\mathrm{T}}$ and $\overline{\boldsymbol{Z}} = \sum_{k=1}^{K} \boldsymbol{Z}_k/K$. For real measurements, the ED compares

$$\mathrm{ED} = \frac{N-d}{d} \cdot \frac{\mathrm{Tr}(\overline{\boldsymbol{Y}}_{\mathrm{T}} \overline{\boldsymbol{Y}}_{\mathrm{T}}^{\mathrm{T}})}{\mathrm{Tr}(\overline{\boldsymbol{Z}}\,\overline{\boldsymbol{Z}}^{\mathrm{T}})} \tag{2.13}$$

with a threshold τ_{ED}, where the presence of a defect is declared if $\mathrm{ED} > \tau_{\mathrm{ED}}$. The above test statistic has an SNR interpretation. The numerator in (2.13) is simply the sum of squared magnitudes of the mean data $\overline{\boldsymbol{Y}}_{\mathrm{T}}$, which is an estimate of the overall power in the window under test. Similarly, the denominator in (2.13) is the sum of squared magnitudes of the (mean) noise-only data $\overline{\boldsymbol{Z}}$, which is an estimate of the noise power. Note that the ED does not account

for noise correlation. Under $\mathcal{H}_0$ and if the noise is white, ED is distributed as

$$\text{ED} \sim F(md, m(N-d)), \tag{2.14}$$

where $F(p, q)$ denotes the F distribution with parameters p and q. For complex measurements, the mean-data energy detector follows by replacing "^{T}" in (2.13) with "^{H}"; then the distribution of ED under $\mathcal{H}_0$ becomes ED $\sim F(2md, 2m(N-d))$.

CHAPTER 3. RESULTS

3.1 Introduction

We apply the proposed methods to simulated eddy-current, experimental ultrasonic C-scan, and X-ray data and demonstrate their superior performance compared to the Mean-Data Energy detectors which neglect noise correlation.

3.2 Simulated Eddy-Current Data

We consider a simulation example with $K = 10$ trials. Figure 3.1(a) shows a magnitude plot of low-noise experimental eddy-current impedance measurements in a sample containing two realistic defects, where each pixel corresponds to a measurement location. The data was collected by scanning the testpiece surface columnwise (parallel to the y axis). To model liftoff variations, we added correlated complex Gaussian noise using autoregressive model AR(1) as follows:

$$x(n) = ax(n-1) + \xi(n), \quad n = 0, 1, \ldots, M-1 \tag{3.1}$$

where $x(n)$ are correlated noise, $\xi(n)$ are i.i.d. complex Gaussian noise having zero mean and variance σ^2, and $x(0) = \xi(0)$. Here, M denotes the size of a vector and a is a constant chosen to satisfy $0 \leq a < 1$. We assume that the noise is correlated along y direction (i.e. between rows) and uncorrelated along x direction (i.e. independent columns). The $M \times M$ covariance matrix of a column vector $\boldsymbol{x} = [x(0)\ x(1)\ \ldots\ x(M-1)]^T$ is symmetric Toeplitz, see [13, Ch.

2.5], and is given by

$$R_x = \frac{\sigma^2}{1-a^2}\begin{bmatrix} 1 & a & a^2 & \dots & a^{M-1} \\ a & 1 & a & \dots & a^{M-2} \\ a^2 & a & 1 & \dots & a^{M-3} \\ \vdots & \vdots & \vdots & \ddots & \vdots \\ a^{M-1} & a^{M-2} & a^{M-3} & \dots & 1 \end{bmatrix}, \tag{3.2}$$

In the experiment, we chose $a = 0.9$ and σ^2 corresponding to the approximate signal to noise ratio (SNR) of -10 db. The approximate SNR is given by

$$\text{SNR} \approx 10 \cdot \log_{10}\left(\frac{E^2}{\sigma_c^2}\right) \tag{3.3}$$

where E^2 is the energy (magnitude squared) average over the area of the true defects and σ_c^2 is the diagonal element of the covariance matrix in (3.2), i.e. $\sigma_c^2 = \sigma^2/(1-a^2)$. Matrices $\boldsymbol{Z}_k$, $k = 1, 2, \dots, 10$ were generated using noise-only regions $\boldsymbol{R}_k$. Windows $\boldsymbol{Y}_{\text{T},k}$ of size $m \times d = 10 \times 10$ were swept across the noisy images, as shown in Figure 3.1(b). Figure 3.2 shows the impedance magnitudes averaged over 10 trials. For each location of the window, we computed the (logarithms of)

- the proposed GLR test statistic in (2.4) and
- the mean-data energy detector for white noise in (2.13),

see Figure 3.3. The results of the GLR and ED detectors are shown in Figure 3.4. For the probability of false alarms $P_{\text{FA}} = 1\%$, the GLR threshold was computed using (2.6) and the ED threshold was computed by utilizing (2.14). Black pixels correspond to the test values larger than the threshold. Clearly, the proposed GLR detector, which accounts for noise correlation, outperforms the mean-data energy detector, which breaks down in this scenario.

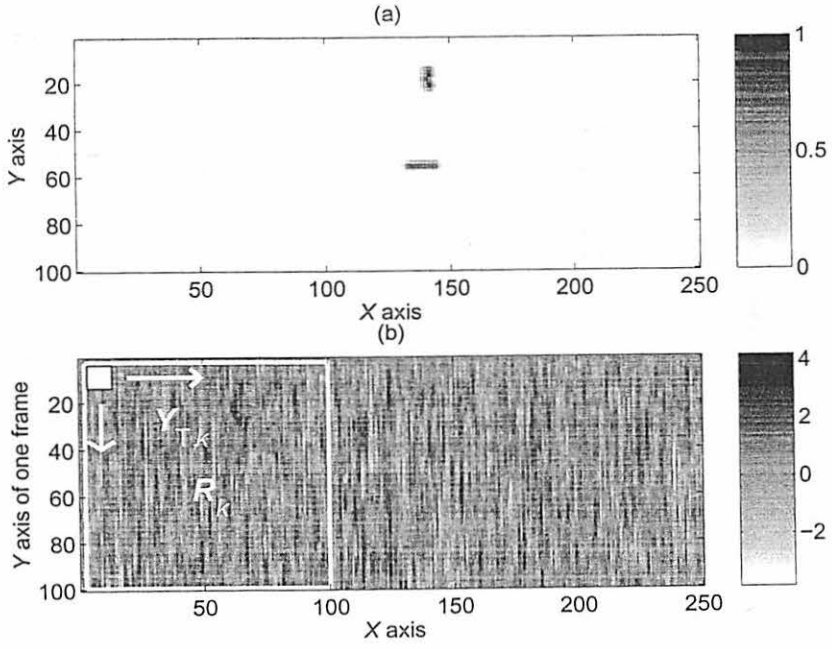

Figure 3.1 (a) Magnitude plot of low-noise eddy-current measurements with peak value normalized to one and (b) a sweeping window $\boldsymbol{Y}_{\mathrm{T},k}$ and a noise-only region $\boldsymbol{R}_k$ shown over noisy measurements for one trial.

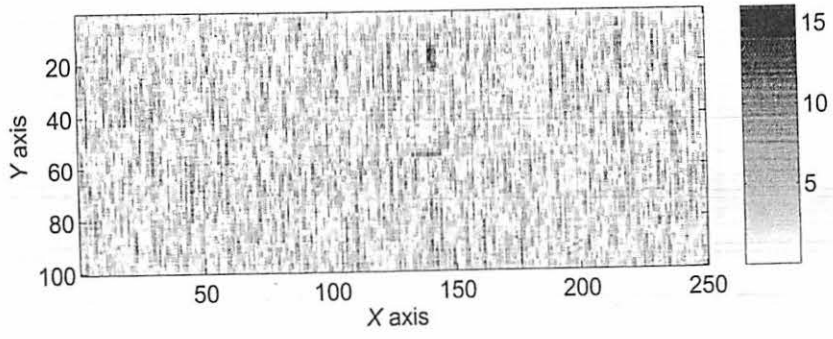

Figure 3.2 Magnitude plot of average data.

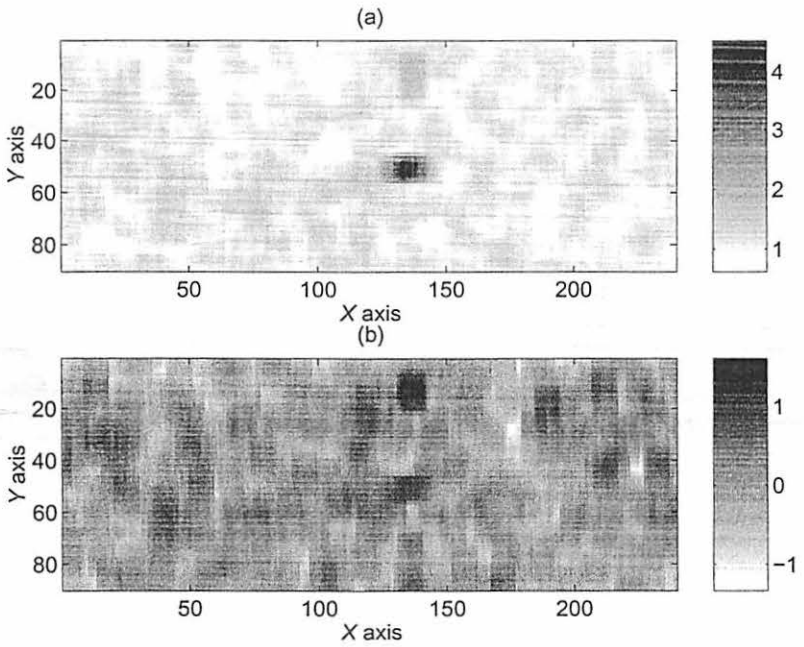

Figure 3.3 Logarithms of (a) the proposed GLR test statistic and (b) the classical ED for multiple trials.

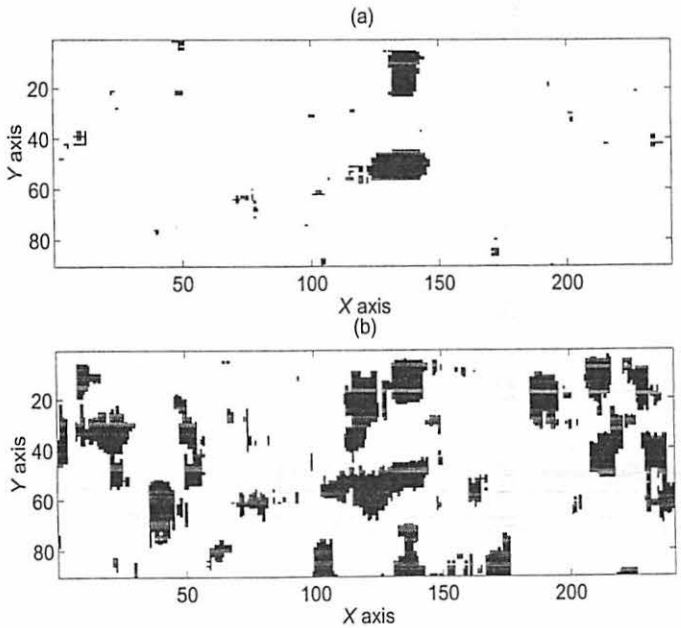

Figure 3.4 (a) GLR detector and (b) energy detector for multiple trials, $P_{\mathrm{FA}} = 1\%$.

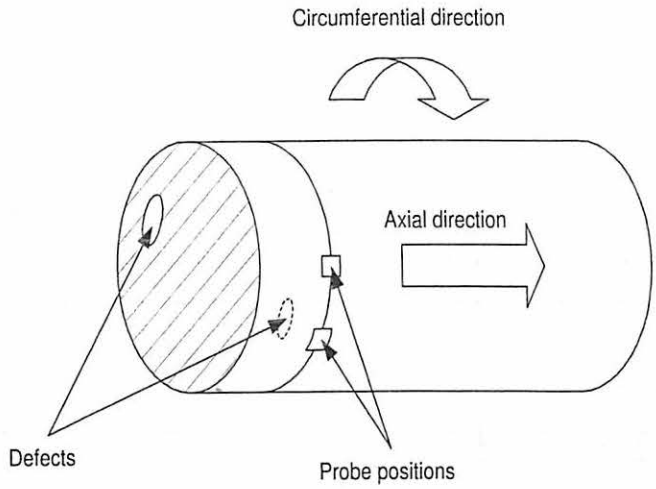

Figure 3.5 Rotating probe directions over Ti 6-4 billet.

3.3 Experimental Ultrasonic Data

We applied the GLR and ED tests to ultrasonic C-scan data from an inspection of a cylindrical Ti 6-4 billet. The data was collected in a single experiment by moving a probe along the axial direction and scanning the billet along the circumferential direction at each axial position, see Figure 3.5. The image of the measurements is shown in Figure 3.6 in which the boxes in Figure 3.6(a) indicate true defect locations. The vertical coordinate is proportional to rotation angle and the horizontal coordinate to axial position. For the ultrasonic data,

- a measurement at each location is determined from the difference of the maximum and minimum values in time series of a testing ultrasonic signal and
- the defect signal level cannot be smaller than the noise level.

This provides a constraint that all elements of X are non-negative when the noise mean is subtracted. The test statistics under this scenario are given by

$$\text{GLR} = \frac{|\widehat{R}|}{\min\limits_{X \succeq 0} |(1/N) \cdot [ZZ^T + (Y_T - X)(Y_T - X)^T]|} \tag{3.4}$$

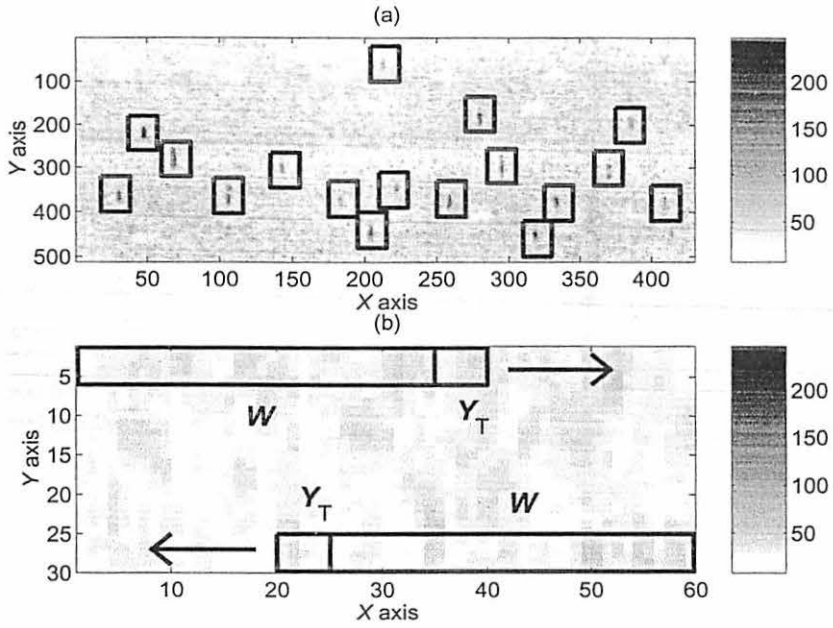

Figure 3.6 (a) Magnitude plot of ultrasonic C-scan data with 17 defects and (b) sweeping window $\boldsymbol{Y}_{\mathrm{T}}$ and a noise-only region $\boldsymbol{W}$ shown over ultrasonic C-scan data.

for the GLR test and

$$\mathrm{ED} = \frac{N-d}{d} \cdot \frac{\mathrm{Tr}(\boldsymbol{Y}_{\mathrm{T}}\boldsymbol{Y}_{\mathrm{T}}^{\mathrm{T}})}{\min\limits_{\boldsymbol{X}\succeq 0} \mathrm{Tr}[\boldsymbol{Z}\boldsymbol{Z}^{T} + (\boldsymbol{Y}_{\mathrm{T}} - \boldsymbol{X})(\boldsymbol{Y}_{\mathrm{T}} - \boldsymbol{X})^{T}]} \tag{3.5a}$$

$$= \frac{N-d}{d} \cdot \frac{\mathrm{Tr}(\boldsymbol{Y}_{\mathrm{T}}\boldsymbol{Y}_{\mathrm{T}}^{\mathrm{T}})}{\mathrm{Tr}[\boldsymbol{Z}\boldsymbol{Z}^{T} + (\boldsymbol{Y}_{\mathrm{T}} - \boldsymbol{Y}_{\mathrm{T}}^{+})(\boldsymbol{Y}_{\mathrm{T}} - \boldsymbol{Y}_{\mathrm{T}}^{+})^{T}]} \tag{3.5b}$$

for the energy detector where $\boldsymbol{X} \succeq 0$ denotes that all elements of $\boldsymbol{X}$ are greater than or equal to zero. The estimator of $\boldsymbol{X}$ for the GLR test is determined by minimizing the denumerator in (3.4) and the estimator of $\boldsymbol{X}$ for the energy detector, denoted by $\boldsymbol{Y}_{\mathrm{T}}^{+}$, is obtained by replacing the negative elements of $\boldsymbol{Y}_{\mathrm{T}}$ with zero, see Appendix D. Windows $\boldsymbol{Y}_{\mathrm{T}}$ and $\boldsymbol{W}$ of dimensions 5×5 and 5×35 were swept across the noisy image, as shown in Figure 3.6(a). We selected the window $\boldsymbol{W}$ from the data that was previously tested and declared to contain only noise. Furthermore, we assume that the noise properties are the same for increasing and decreasing y coordinates. Hence, to exploit the stationarity and improve estimation of the noise covariance

Σ, we generate a noise-only matrix $\boldsymbol{Z}$ using both $\boldsymbol{W}$ and a vertically flipped version of $\boldsymbol{W}$. Note that in this case, $m = 5$, $N = 75$, and $d = 5$. (In each tested area, we compute the average of measurements in the region $\boldsymbol{W}$ and subtract it from an observation matrix to obtain the matrices $\boldsymbol{Z}$ and $\boldsymbol{Y}_{\mathrm{T}}$.) We also compared the above detectors to a peak-to-average SNR method based on [15] and used by General Electric (GE) Corporate Research and Development Center for determining the acceptable region of materials. The method compares

$$\mathrm{SNR}_{\mathrm{PA}} = \frac{y_{\mathrm{T,max}} - \overline{y}_{\mathrm{T}}}{z_{\max} - \overline{z}} \tag{3.6}$$

with a threshold τ_{PA} where the acceptance of a region is declared when $\mathrm{SNR}_{\mathrm{PA}}$ is less than or equal to the threshold. Here, $y_{\mathrm{T,max}}$ and $z_{\max}$ denote the maximum values of the testing window $\boldsymbol{Y}_{\mathrm{T}}$ and the noise-only region $\boldsymbol{W}$, respectively. $\overline{y}_{\mathrm{T}}$ and $\overline{z}$ are the average of elements in $\boldsymbol{Y}_{\mathrm{T}}$ and $\boldsymbol{W}$. For each location of the window, we computed the (logarithms of) the proposed GLR test statistic and the energy detector. The windows were swept from left to right and backward as shown in Figure 3.6(b). For the same $\boldsymbol{Y}_{\mathrm{T}}$, denote the GLRs from the first and the second sweeps by GLR_1 and GLR_2, respectively. Similarly, denote the corresponding EDs by ED_1 and ED_2. Figure 3.7 shows $[\ln(\mathrm{GLR}_1) + \ln(\mathrm{GLR}_2)]/2$ and $[\ln(\mathrm{ED}_1) + \ln(\mathrm{ED}_2)]/2$, respectively. The presence of a defect is declared if both GLR_1 and GLR_2 (or ED_1 and ED_2) are greater than a threshold. The detection results are shown in Figure 3.8 for the GLR test and energy detectors, where the threshold was chosen to guarantee the probability of false alarms of 1%. The black pixels correspond to the GLR (or ED) values larger than the threshold. Figure 3.9 shows the detection result using the original GLR test in Chapter 2 designed without the constraint $\boldsymbol{X} \succeq \boldsymbol{0}$. For the peak-to-average SNR method in [15], the windows $\boldsymbol{Y}_{\mathrm{T}}$ and $\boldsymbol{W}$ were swept for one direction from left to right and we computed $\mathrm{SNR}_{\mathrm{PA}}$ for each location of $\boldsymbol{Y}_{\mathrm{T}}$. The detection results for thresholds τ_{PA} = 1.0, 1.5, and 2.0 are shown in Figures 3.10, 3.11, and 3.12, respectively. Clearly, the proposed GLR detector outperforms the original GLR detector, energy detector, and peak-to-average SNR method.

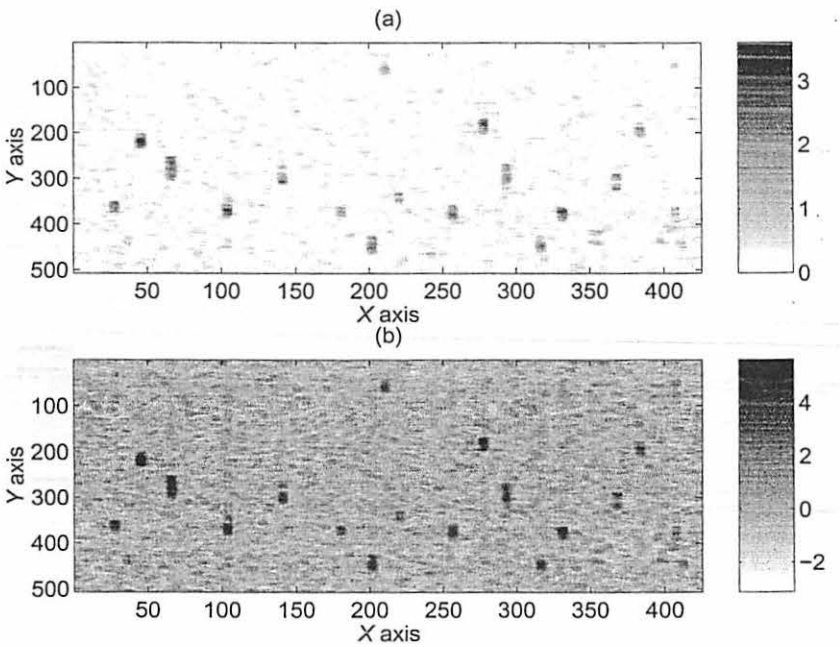

Figure 3.7 Average of logarithms of (a) GLR_1 and GLR_2 and (b) ED_1 and ED_2.

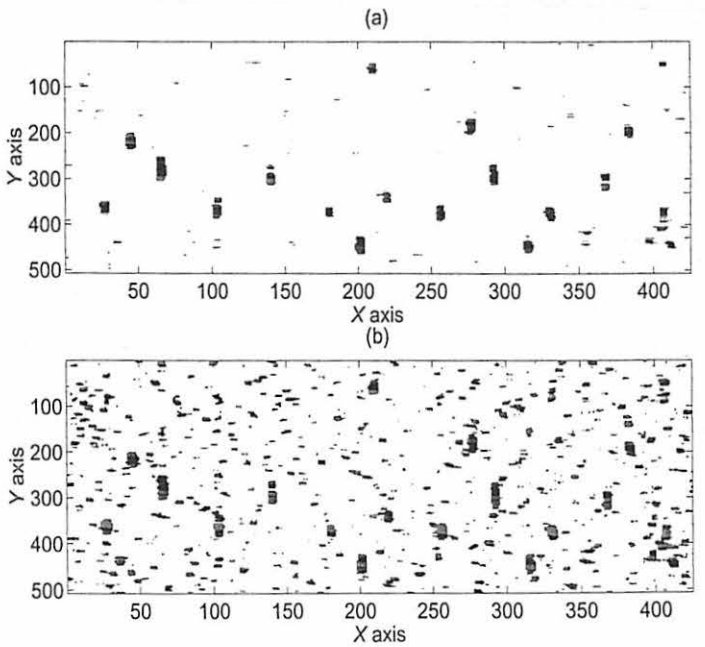

Figure 3.8 (a) GLR detector and (b) energy detector for $P_{\mathrm{FA}} = 1\%$.

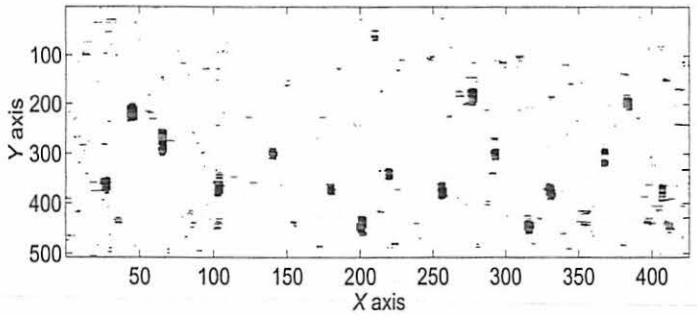

Figure 3.9 GLR detector without the constraint $\boldsymbol{X} \succeq 0$ for $P_{\mathrm{FA}} = 1\%$.

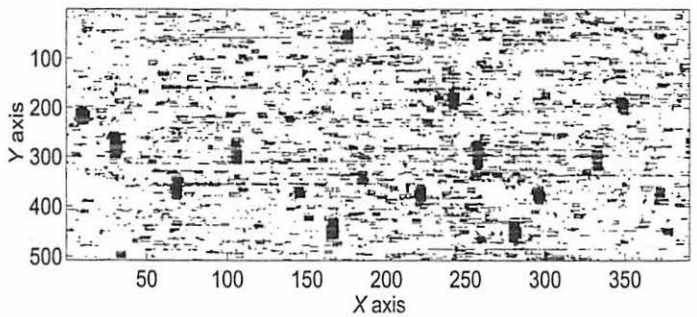

Figure 3.10 Detector using the peak-to-average SNR method for $\tau_{\mathrm{PA}} = 1.0$.

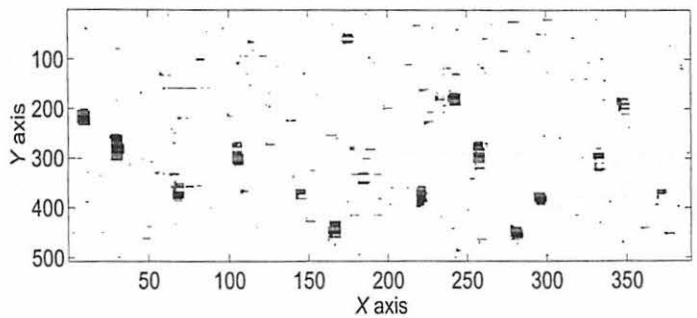

Figure 3.11 Detector using the peak-to-average SNR method for $\tau_{\mathrm{PA}} = 1.5$.

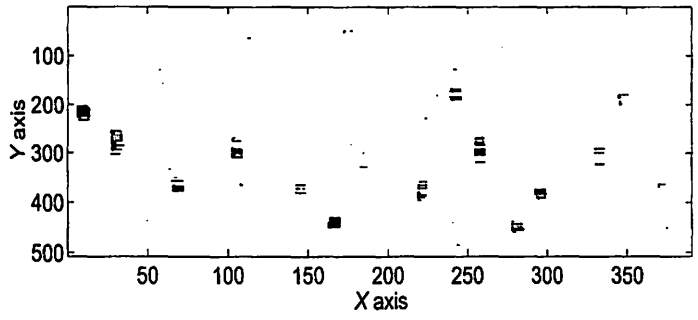

Figure 3.12 Detector using the peak-to-average SNR method for $\tau_{\mathrm{PA}} = 2.0$.

3.4 Experimental X-Ray Data

We applied the GLR and ED tests to experimental X-ray data from inspections of a motor mount with $K = 10$, see Figure 3.13. Figure 3.14(a) shows a low-noise image of the defects, reconstructed using computed tomography (CT) scans and Figure 3.14(b) shows an X-ray image averaged over the 10 trials. At the kth trial (where $k = 1,2, \ldots, 10$), a window $\boldsymbol{Y}_{\mathrm{T},k}$ and a noise-only matrix $\boldsymbol{Z}_k$ of dimensions $m \times d = 5 \times 5$ and $m \times (N - d) = 5 \times 35$ were swept across the noisy images shown in Figure 3.15. For each location of the window, we computed the (logarithms of) the GLR test statistic and the energy detector. The results are illustrated in Figure 3.16 and the detection results are shown in Figure 3.17 for the GLR test and energy detectors, where the threshold was chosen to satisfy the probability of false alarms of 0.1%. As before, black pixels correspond to the GLR (or ED) values larger than the threshold. In this example, the GLR and ED expressions yielded similar results.

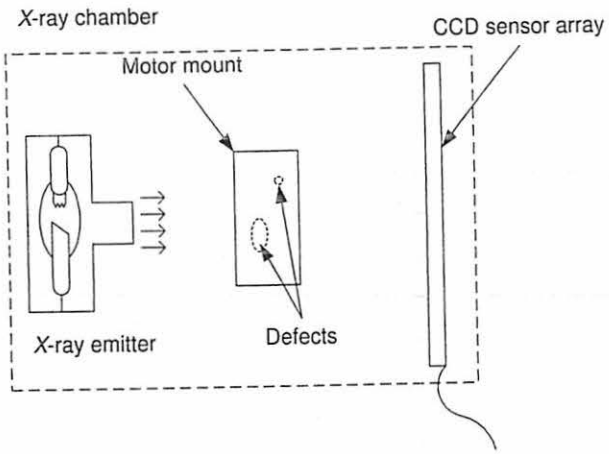

Figure 3.13 X-ray chamber diagram.

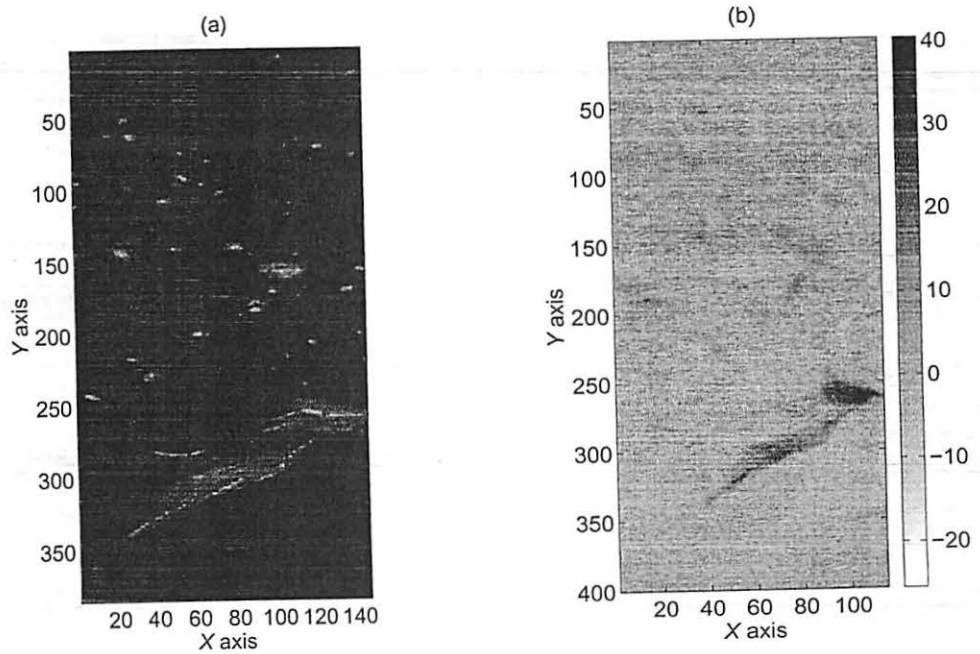

Figure 3.14 (a) Low-noise image of the defects and (b) an X-ray image average over 10 trials.

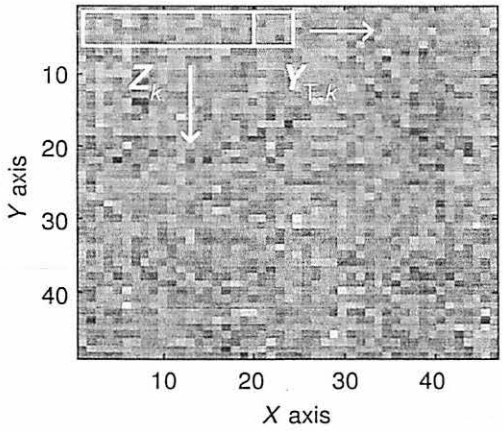

Figure 3.15 Sweeping windows $\boldsymbol{Y}_{\mathrm{T},k}$ and $\boldsymbol{Z}_k$, $k = 1, 2, \ldots, K$ of dimensions $m \times d = 5 \times 5$ and $m \times (N - d) = 5 \times 20$ (respectively) shown over the noisy images.

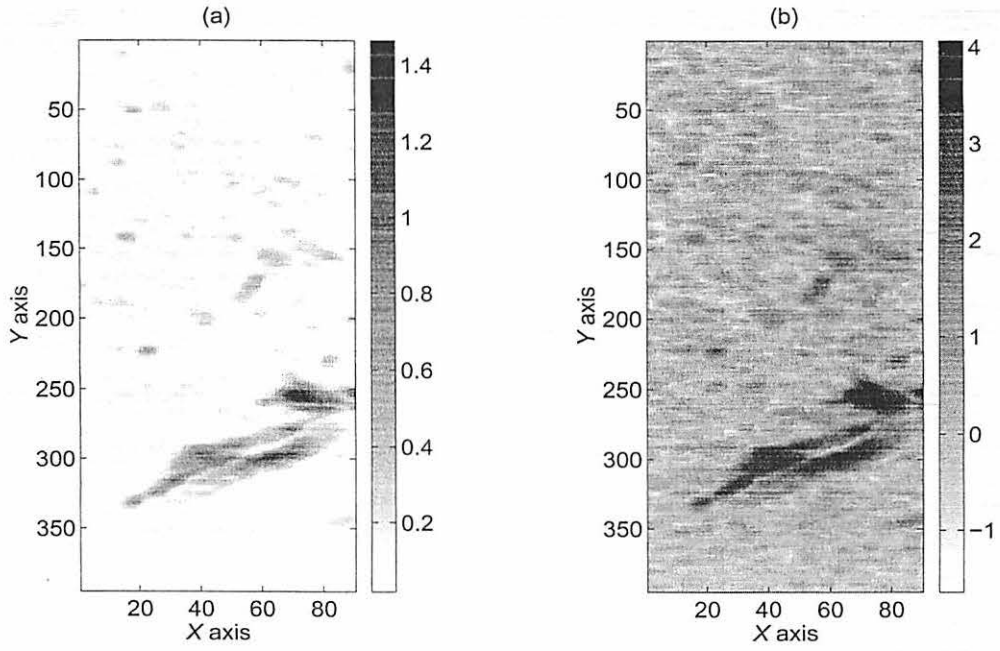

Figure 3.16 (a) ln GLR and (b) ln ED.

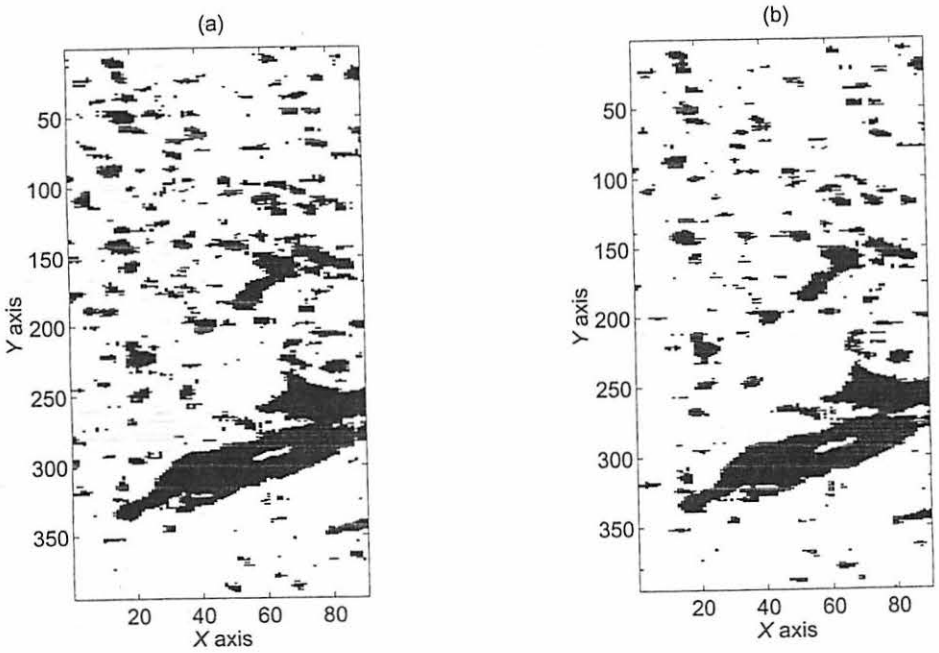

Figure 3.17 (a) GLR detector and (b) energy detector for $P_{\mathrm{FA}} = 0.1\%$.

CHAPTER 4. SUMMARY AND FUTURE WORK

4.1 Conclusion

We developed generalized likelihood ratio tests for NDE defect detection in correlated noise having unknown covariance. The detectors for real and complex data models and their probability distributions were derived under the noise-only scenario. We also designed the detectors for data sets obtained from multiple experiments. In the data models, the noise was assumed to be correlated between rows and independent between columns, i.e. we considered the case when measurement data is collected along the vertical direction at each position of the horizontal direction. We also developed a numerical method for computing the exact distributions of the tests used to determine decision thresholds for specified false-alarm probabilities. The proposed detectors were applied to simulated eddy-current, experimental ultrasonic, and experimental X-ray data and compared with the constant false-alarm rate energy detector and peak-to-average SNR method (for the case of ultrasonic data). The GLR detector outperformed the other methods when model assumptions are satisfied. Otherwise, if the noise correlation is not constant (and the same) in $\boldsymbol{Y}_T$ and $\boldsymbol{Z}$ regions, or if the noise is not Gaussian, the GLR detector may not improve the detection. There are still some problems that remain unsolved such as the optimum sizes of the testing windows $\boldsymbol{Y}_{\mathrm{T}}$ and the noise-only region $\boldsymbol{Z}$ corresponding to defect sizes. In addition, we considered the noise only for the Gaussian cases which are not always true in practise and it may not be possible to find the numerical form of a true distribution in that case. Furthermore, the data model can be designed for more general cases such as the model in Appendix A in which $\boldsymbol{A}$ and Φ are known. All of these problems require further research.

4.2 Future Work

The further work will include

- developing the GLR detector for a more general signal-mean model,
- accounting for noise correlation between columns of the data matrices, and
- developing a method to improve the detector and remove false alarms.

In the following section, we present an example method using maximum a posteriori (MAP) estimation and hidden Markov models to eliminate false alarms caused by the GLR detector.

4.2.1 MAP Estimation and Classification Using Hidden Markov Models

We plan to model the result obtained from the GLR test using hidden Markov models (HMMs), in which the observations are assumed to form a noisy realization of an underlying random field that has a simple structure with Markovian dependence. Here, the random field describes the defect signal and our goal is to estimate it from noisy measurements. The underlying spatial statistical methodology incorporates the spatial locations of the measurements into the statistical analysis, which is important in the scenario where the same defect affects the measurements at multiple spatial locations (as is almost always the case in practical applications). We focus on a statistical approach that models the random field at a particular measurement location in terms of the field values at neighboring locations.

Assume that K spatially distributed measurements y_k, $k = 1, 2, \ldots, K$ have been collected. We approach the problem of modeling y_k by breaking it into two stages: We assume that

- y_k are conditionally independent random vectors with probability distributions $p_{y_k|\beta_k}(y_k|\beta_k; \upsilon)$ describing the *data (measurement-error) model* and
- β_k, $k = 1, 2, \ldots, K$ form a *Markov random field* describing the *process model.*

Consequently, y_k follow a *hidden Markov model* [16, 17]. This model can account for both discrete and continuous random fields and measurements. We concentrate on *conditionally specified* MRFs, where a consistent specification of conditional distributions is required to ensure that the joint distribution of $\beta_1, \beta_2, \ldots, \beta_K$ is well-defined, see e.g. [18, 19].

4.2.2 MRF Model Examples

4.2.2.1 Discrete MRF for Classification

Suppose that each measurement k is associated to one of Ξ classes and let us model $\beta_k \in \{1, 2, \ldots, \Xi\}$ as a discrete MRF. For example, choose the conditional probability that measurement k belongs to a class $\xi \in \{1, 2, \ldots, \Xi\}$ given the class assignments at the neighboring measurements as

$$P[\beta_k = \xi \mid \mathcal{N}(k)] = \exp\left[b_\xi - \sum_{l \in \mathcal{N}(k)} \sum_{d=1}^{\Xi} \delta_{\xi,d}\, c_{k,l}\right], \tag{4.1}$$

where b_ξ, $\delta_{\xi,d}$, and $c_{k,l}$ are the calibration parameters that satisfy $\delta_{\xi,d} = \delta_{d,\xi}$, $\delta_{\xi,\xi} = 0$, $c_{k,l} = c_{l,k}$, and $c_{k,k} = 0$. Also, $c_{k,l} = 0$ if the measurements k and l are not coming from neighboring locations $\mathcal{N}(k)$, which is the *Markovian assumption*. Here the parameters $\delta_{\xi,d}$ and $c_{k,l}$ describe the inter-class relationships and spatial Markov structure of the random field, respectively. The coefficients $c_{k,l}$ may be modeled as functions of the distances between measurement locations. For example, denote the kth and lth measurement locations by $\boldsymbol{r}_k$ and $\boldsymbol{r}_l$ and assume that the random field is isotropic; then we may model $c_{k,l}$ as a decreasing function of the squared distance $(\boldsymbol{r}_k - \boldsymbol{r}_l)^T(\boldsymbol{r}_k - \boldsymbol{r}_l)$ (see [19]), e.g.

$$c_{k,l} = c_{k,l}(\boldsymbol{r}_k - \boldsymbol{r}_l) = \begin{cases} \eta\left[d^2_{\text{MIN}}/(\boldsymbol{r}_k - \boldsymbol{r}_l)^T(\boldsymbol{r}_k - \boldsymbol{r}_l)\right]^\gamma, & (\boldsymbol{r}_k - \boldsymbol{r}_l)^T(\boldsymbol{r}_k - \boldsymbol{r}_l) \le d^2, \\ 0, & (\boldsymbol{r}_k - \boldsymbol{r}_l)^T(\boldsymbol{r}_k - \boldsymbol{r}_l) > d^2, \end{cases} \tag{4.2}$$

where $d^2_{\text{MIN}} = \min_{\forall k,l\ k \neq l}\{(\boldsymbol{r}_k - \boldsymbol{r}_l)^T(\boldsymbol{r}_k - \boldsymbol{r}_l)\}$ and η and γ are the calibration parameters. Here, the *neighborhood of a measurement* k consists of all the measurements that are collected

within the *cutoff distance* d from that measurement, and is denoted by $\mathcal{N}(k)$. Note also that the calibration parameters should be chosen to ensure that (4.1) is a valid probability mass function. In the simple case where $c_{k,l}$ is the neighborhood index (i.e. it equals one if $l \in \mathcal{N}(k)$ and zero otherwise) and if classes are *interchangeable* (i.e. $\delta_{\xi,d} = \delta$ does not depend on ξ and d), this model simplifies to the isotropic Potts model [20]:

$$P[\beta_k = \xi \mid \mathcal{N}(k)] = \exp[\delta \cdot u_k(\xi)] \Big/ \Big\{ \sum_{d=1}^{\Xi} \exp[\delta \cdot u_k(d)] \Big\}, \tag{4.3}$$

where $u_k(\xi)$ is the number of neighbors of node k that belong to class ξ. In the above model, equal weight is given to the evidence from each neighbor. Clearly, for positive δ, this model favors probabilistically those classification results where neighboring locations belong to the same class.

4.2.2.2 Distributed MAP Estimation

We wish to estimate the MRF $\boldsymbol{\beta} = [\beta_1, \beta_2, \ldots, \beta_K]^T$ from the observations y_k, $k = 1, 2, \ldots, K$, where the model parameters are assumed to be known. We compute the MAP estimates of $\boldsymbol{\beta}$ by performing the following steps for each k:

(MAP1) collect the current estimates of β_l, $l \in \mathcal{N}(k)$ from the neighborhood of k and

(MAP2) update the estimate of β_k by maximizing the "local" (conditional) MAP objective function:

$$L_{\text{MAP},k}\big(\beta_k \mid \beta_l \in \mathcal{N}(k); \boldsymbol{\upsilon}, \boldsymbol{\theta}\big) = \ln[p_{\upsilon_k|\beta_k}(\boldsymbol{y}_k|\beta_k; \boldsymbol{\upsilon})] + \ln p_{\beta_k|\mathcal{N}(k)}\big(\beta_k|\mathcal{N}(k); \boldsymbol{\theta}\big) \tag{4.4}$$

with respect to β_k.

Here, $\boldsymbol{\upsilon}$ and $\boldsymbol{\theta}$ are the data and MRF model parameters, respectively. (For example, $\boldsymbol{\theta} = [\eta, \gamma, d, \delta_{\xi,d}, b_\xi]^T$ in the model (4.1)–(4.2).) Applying (MAP1)–(MAP2) to each k in turn yields

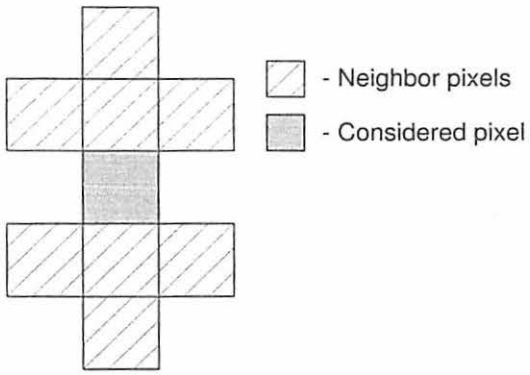

Figure 4.1 Neighborhood of a pixel.

a single cycle of an iteration which continues until convergence. In general, this iteration will converge to a local maximum of the "global" MAP objective function:

$$L_{\text{MAP}}(\boldsymbol{\beta}) = \Big(\sum_{k=1}^{K} \ln[p_{y_k|\beta_k}(\boldsymbol{y}_k|\beta_k; \boldsymbol{\upsilon})] \Big) + \ln[p_{\beta}(\boldsymbol{\beta}; \boldsymbol{\theta})]. \tag{4.5}$$

The above iteration can be initialized using the maximum likelihood (ML) estimates $\widehat{\beta}_{\text{ML},k} = \arg\max_{\beta_k} \ln[p_{y_k|\beta_k}(y_k|\beta_k; \boldsymbol{\upsilon})]$ which ignore the underlying neighborhood structure. The proposed MAP algorithm is closely related to the *iterated conditional modes* (ICM) in [20] for image analysis, see also [16, 19, 21]. However, the neighborhood models developed for image processing applications are fairly simple. Due to possibly non-uniformly distributed meausrements, we allow for more complex neighborhood correlation models, such as (4.2).

4.2.2.3 Simulation Example

We now apply the above MAP method to the experimental ultrasonic data in Chapter 3 to remove false alarms caused by the GLR detector and compare it to the original result of the GLR detector. We use the isotropic Potts model in (4.3) with neighborhood defined by surrounding measurement locations (pixels) as shown in Figure 4.1. Our goal is to classify the noisy data into $\Xi = 2$ classes. Hence, $\beta_k \in \{0, 1\}$ where one class represents the presence of a defect

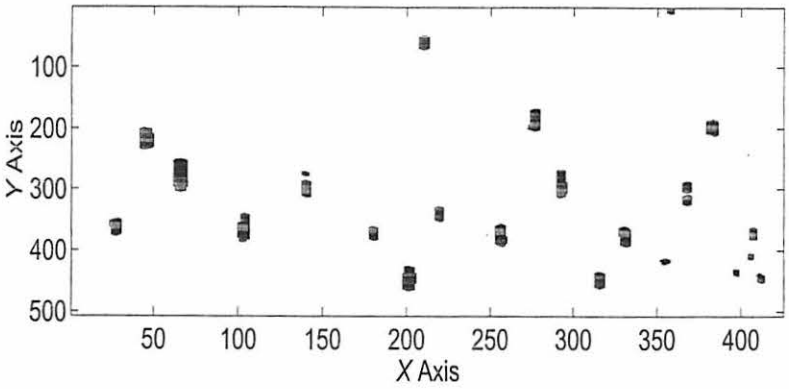

Figure 4.2 MAP detector.

whereas the other represents the absence of defects. We use the following data models,

$$\begin{aligned}(y_k|\beta_k = 0, \boldsymbol{\upsilon}) &\sim \mathcal{N}(\mu_0, \sigma_0^2) \\ (y_k|\beta_k = 1, \boldsymbol{\upsilon}) &\sim \mathcal{N}(\mu_1, \sigma_1^2),\end{aligned}$$

where $\mathcal{N}(\mu, \sigma^2)$ denotes the Gaussian distribution with mean μ and variance σ^2. Here, the data model parameters are $[\mu_0, \mu_1, \sigma_0^2, \sigma_1^2]^T$. Since $\boldsymbol{\upsilon}$ is not known in general, we propose iterating between the MAP and ML clustering algorithms, see [22, Ch. 22], where

- the ML clustering algorithm is used to estimate $\boldsymbol{\upsilon}$ and
- the MAP algorithm is used to classify pixels into two classes.

The above iteration is initialized using the GLR detector result in Figure 3.8(a). (Upon convergence of the MAP step, we use the obtained pixel classification to estimate the prior probabilities for the next ML clustering step.) In the following example, we apply the above iterative algorithm to the GLR test result in Chapter 3, see Figure 3.6(a) and 3.7(a), and then compare it with the original GLR detector in Figure 3.8(a). The result is shown in Figure 4.2 for $\delta = 4.5$. Obviously, the above method can eliminate almost all false alarms caused by the GLR detector.

APPENDIX A. GENERALIZED MULTIVARIATE ANALYSIS OF VARIANCE

Problem Formulation

In this section, we show the derivation of the Generalized Likelihood Ratio (GLR) test for the detection problem in Chapter 2 using Generalized Multivariate Analysis of Variance (GMANOVA). We consider the following measurement model

$$\boldsymbol{Y} = \boldsymbol{A}\boldsymbol{X}\boldsymbol{\Phi} + \boldsymbol{E} \tag{A.1}$$

where $\boldsymbol{Y}$ is an $m \times \widetilde{N}$ observation matrix and $\boldsymbol{X}$ denotes an unknown matrix with the size of $j \times d$. $\boldsymbol{A}$ and $\boldsymbol{\Phi}$ are known matrices with the size of $m \times j$ and $d \times \widetilde{N}$, respectively. Here, $\boldsymbol{E}$ denotes an $m \times \widetilde{N}$ matrix of random variables where the columns of $\boldsymbol{E}$ are independent, identically distributed (i.i.d.) zero-mean Gaussian vectors having an unknown covariance $\boldsymbol{\Sigma}$. We wish to detect the presence of $\boldsymbol{X}$: i.e. testing null hypothesis

$$\mathcal{H}_0 : \boldsymbol{X} = 0$$

versus the alternative

$$\mathcal{H}_1 : \boldsymbol{X} \neq 0.$$

GLR Test for Real Data

For a real data scenario, under the null hypothesis, the joint probability density function (PDF) of the elements of data array $\boldsymbol{Y}$ is given by

$$f_0(\boldsymbol{Y};\boldsymbol{\Sigma}) = \frac{1}{|2\pi\boldsymbol{\Sigma}|^{\tilde{N}/2}} \cdot \exp\Big[-\frac{1}{2}\mathrm{Tr}\big(\boldsymbol{Y}^T\boldsymbol{\Sigma}^{-1}\boldsymbol{Y}\big)\Big] \tag{A.2}$$

and the joint PDF under the alternate hypothesis is given by

$$f_1(\boldsymbol{Y};\boldsymbol{\Sigma}) = \frac{1}{|2\pi\boldsymbol{\Sigma}|^{\tilde{N}/2}} \cdot \exp\Big\{-\frac{1}{2}\mathrm{Tr}\Big[\big(\boldsymbol{Y}-\boldsymbol{A}\boldsymbol{X}\boldsymbol{\Phi}\big)^T\boldsymbol{\Sigma}^{-1}\big(\boldsymbol{Y}-\boldsymbol{A}\boldsymbol{X}\boldsymbol{\Phi}\big)\Big]\Big\}. \tag{A.3}$$

where Tr $(\cdot)$ denotes trace, the subscript "^{T}" represents transpose, and $|\cdot|$ denotes the determinant. The maximum likelihood (ML) estimate of covariance matrices under $\mathcal{H}_0$ and $\mathcal{H}_1$ can be determined using the following equations:

$$\widehat{\boldsymbol{\Sigma}}_0 = \frac{1}{\tilde{N}}\boldsymbol{Y}\boldsymbol{Y}^T \tag{A.4a}$$

$$\widehat{\boldsymbol{\Sigma}}_1 = \frac{1}{\tilde{N}}(\boldsymbol{Y}-\boldsymbol{A}\boldsymbol{X}\boldsymbol{\Phi})(\boldsymbol{Y}-\boldsymbol{A}\boldsymbol{X}\boldsymbol{\Phi})^T \tag{A.4b}$$

The test statistic is, by definition,

$$\frac{\max\limits_{\boldsymbol{\Sigma},\boldsymbol{X}} f_1(\boldsymbol{Y};\boldsymbol{\Sigma},\boldsymbol{X})}{\max\limits_{\boldsymbol{\Sigma}} f_0(\boldsymbol{Y};\boldsymbol{\Sigma})} = \frac{\max\limits_{\boldsymbol{X}} f_1(\boldsymbol{Y};\widehat{\boldsymbol{\Sigma}}_1(\boldsymbol{X}),\boldsymbol{X})}{f_0(\boldsymbol{Y};\widehat{\boldsymbol{\Sigma}}_0)}, \tag{A.5}$$

which is equivalent to a test based on

$$\text{Test statistic} \equiv \frac{|\widehat{\boldsymbol{\Sigma}}_0|}{\min\limits_{\boldsymbol{X}}|\widehat{\boldsymbol{\Sigma}}_1|}. \tag{A.6}$$

Since in this case, it is a composite hypothesis testing, i.e. $\boldsymbol{X}$ and $\boldsymbol{\Sigma}$ are unknown under the alternative hypothesis, we may use the GLR test as the suboptimum solution, see [6]. In general,

we assume that the rank of $\boldsymbol{A}$ is $j \leq m$ and the rank of Φ is $d \leq \widetilde{N}$. Since both $\boldsymbol{A}$ and Φ are full rank, $\boldsymbol{A}^T\boldsymbol{A}$ and $\Phi\Phi^T$ are positive definite and non-singular. The GLR in [6] for full rank $\boldsymbol{A}$ and Φ is expressed as follows:

$$\text{GLR} = \frac{|\widehat{\boldsymbol{R}}_{\phi\phi} - \widehat{\boldsymbol{R}}_{y\phi}^T \boldsymbol{\mathcal{W}} \widehat{\boldsymbol{R}}_{y\phi}|}{|\widehat{\boldsymbol{S}}_{\phi|y}|} \tag{A.7}$$

where

$$\begin{aligned}
\boldsymbol{\mathcal{W}} &= \widehat{\boldsymbol{R}}_{yy}^{-1} - \widehat{\boldsymbol{R}}_{yy}^{-1}\boldsymbol{A}[\boldsymbol{A}^T\widehat{\boldsymbol{R}}_{yy}^{-1}\boldsymbol{A}]^{-1}\boldsymbol{A}^T\widehat{\boldsymbol{R}}_{yy}^{-1}, && \text{(A.8a)}\\
\widehat{\boldsymbol{S}}_{\phi|y} &= \widehat{\boldsymbol{R}}_{\phi\phi}^{-1} - \widehat{\boldsymbol{R}}_{y\phi}^T\widehat{\boldsymbol{R}}_{yy}^{-1}\widehat{\boldsymbol{R}}_{y\phi}, && \text{(A.8b)}\\
\widehat{\boldsymbol{R}}_{\phi\phi} &= \frac{1}{\widetilde{N}}\Phi\Phi^T, && \text{(A.8c)}\\
\widehat{\boldsymbol{R}}_{y\phi} &= \frac{1}{\widetilde{N}}\boldsymbol{Y}\Phi^T, \text{ and} && \text{(A.8d)}\\
\widehat{\boldsymbol{R}}_{yy} &= \widehat{\Sigma}_0 = \frac{1}{\widetilde{N}}\boldsymbol{Y}\boldsymbol{Y}^T. && \text{(A.8e)}
\end{aligned}$$

For the model in Chapter 2, we consider the case that the experiment in which the measurements are collected is repeated K times. The observation matrix $\boldsymbol{Y}$ can be presented by the series of individual observation matrices $\boldsymbol{Y}_k$ in K experiments. Here, the matrix $\boldsymbol{Y}_k$ of size $m \times N$ consists of two parts, the testing window $\boldsymbol{Y}_{\text{T},k}$ and noise-only region $\boldsymbol{Z}_k$. In Chapter 2, we model the framework using the following configuration.

$$\begin{aligned}
\widetilde{N} &= NK, && \text{(A.9a)}\\
\boldsymbol{A} &= \boldsymbol{I}_m, && \text{(A.9b)}\\
\Phi &= [0, \boldsymbol{I}_d| \ \cdots \ | 0, \boldsymbol{I}_d]_{d\times NK}, \text{ and} && \text{(A.9c)}\\
\boldsymbol{Y} &= [\boldsymbol{Y}_1| \ \cdots \ | \boldsymbol{Y}_k]_{m\times NK} && \text{(A.9d)}\\
&= [\boldsymbol{Z}_1, \boldsymbol{Y}_{\text{T},1}| \ \cdots \ | \boldsymbol{Z}_K, \boldsymbol{Y}_{\text{T},K}]_{m\times NK}, && \text{(A.9e)}
\end{aligned}$$

where $\boldsymbol{I}_m$ and $\boldsymbol{I}_d$ are the identity matrices of size $m \times m$ and $d \times d$, respectively. Here, "0" denotes a zero matrix of size $d \times N - d$. By applying the parameters above, the test statistic in (A.7) can be reduced to

$$\text{GLR} = \frac{|\widehat{\boldsymbol{R}}_{yy}|}{|\widehat{\boldsymbol{R}}_{yy} - (1/N) \cdot \overline{\boldsymbol{Y}}_{\text{T}} \overline{\boldsymbol{Y}}_{\text{T}}^{\,T}|} \tag{A.10a}$$

$$= \frac{1}{|\boldsymbol{I}_d - (1/N) \cdot \overline{\boldsymbol{Y}}_{\text{T}}^{\,T} \widehat{\boldsymbol{R}}_{yy}^{-1} \overline{\boldsymbol{Y}}_{\text{T}}|} \tag{A.10b}$$

where

$$\widehat{\boldsymbol{R}}_{yy} = \frac{1}{NK} \sum_{k=1}^{K} (\boldsymbol{Y}_{\text{T},k} \boldsymbol{Y}_{\text{T},k}^{\,T} + \boldsymbol{Z}_k \boldsymbol{Z}_k^{\,T}) \text{ and} \tag{A.11a}$$

$$\overline{\boldsymbol{Y}}_{\text{T}} = \frac{1}{K} \sum_{k=1}^{K} \boldsymbol{Y}_{\text{T},k}. \tag{A.11b}$$

We may also rearrange the above test statistic in the form of

$$\text{GLR} = |\boldsymbol{I}_d + \boldsymbol{V}^T \boldsymbol{T}^{-1} \boldsymbol{V}| \tag{A.12a}$$

$$= \frac{|\boldsymbol{T} + \boldsymbol{V}\boldsymbol{V}^T|}{|\boldsymbol{T}|} \tag{A.12b}$$

where

$$\boldsymbol{T} = \widehat{\boldsymbol{R}}_{yy} - \frac{1}{N} \overline{\boldsymbol{Y}}_{\text{T}} \overline{\boldsymbol{Y}}_{\text{T}}^{\,T} \tag{A.13a}$$

$$= \frac{1}{NK} \sum_{k=1}^{K} \left[(\boldsymbol{Y}_{\text{T},k} - \overline{\boldsymbol{Y}}_{\text{T}})(\boldsymbol{Y}_{\text{T},k} - \overline{\boldsymbol{Y}}_{\text{T}})^T + \boldsymbol{Z}_k \boldsymbol{Z}_k^{\,T} \right] \tag{A.13b}$$

$$= (\boldsymbol{Y} - \overline{\boldsymbol{Y}}_{\text{T}} \boldsymbol{\Phi})(\boldsymbol{Y} - \overline{\boldsymbol{Y}}_{\text{T}} \boldsymbol{\Phi})^T \text{ and} \tag{A.13c}$$

$$\boldsymbol{V} = \frac{1}{\sqrt{N}} \overline{\boldsymbol{Y}}_{\text{T}}. \tag{A.13d}$$

Since $\boldsymbol{V}$ and $\boldsymbol{T}$ are respectively in the form of sample mean and covariance, it is clear that they are unconditionally independent. We may express $\boldsymbol{T}$ in terms of Gaussian array $\boldsymbol{W}$ of

dimension $j \times NK + j - m - d$ as follows:

$$T = \overline{W} W^T. \tag{A.14}$$

Note that in this special case, $j = m$.

GLR Test for Complex Data

For a complex data scenario, under the null hypothesis, the joint PDF of the elements of data array $\boldsymbol{Y}$ is given by

$$f_0(\boldsymbol{Y}; \boldsymbol{\Sigma}) = \frac{1}{|\pi \boldsymbol{\Sigma}|^{\tilde{N}}} \cdot \exp\Big[- \mathrm{Tr}\big(\boldsymbol{Y}^H \boldsymbol{\Sigma}^{-1} \boldsymbol{Y}\big)\Big] \tag{A.15}$$

and the joint PDF under the alternate hypothesis is given by

$$f_1(\boldsymbol{Y}; \boldsymbol{\Sigma}) = \frac{1}{|\pi \boldsymbol{\Sigma}|^{\tilde{N}}} \cdot \exp\Big\{ - \mathrm{Tr}\Big[\big(\boldsymbol{Y} - \boldsymbol{A}\boldsymbol{X}\boldsymbol{\Phi}\big)^H \boldsymbol{\Sigma}^{-1} \big(\boldsymbol{Y} - \boldsymbol{A}\boldsymbol{X}\boldsymbol{\Phi}\big)\Big]\Big\}. \tag{A.16}$$

where the superscript "^{H}" represents Hermitian (conjugate) transpose. By applying the same method as in the real data case, the GLR test statistic can be represented by the following equation:

$$\mathrm{GLR} = \frac{|\widehat{\boldsymbol{R}}_{yy}|}{|\widehat{\boldsymbol{R}}_{yy} - (1/N) \cdot \overline{\boldsymbol{Y}}_{\mathrm{T}} \overline{\boldsymbol{Y}}_{\mathrm{T}}^{\,H}|} \tag{A.17a}$$

$$= \frac{1}{|\boldsymbol{I}_d - (1/N) \cdot \overline{\boldsymbol{Y}}_{\mathrm{T}}^{\,H} \widehat{\boldsymbol{R}}_{yy}^{-1} \overline{\boldsymbol{Y}}_{\mathrm{T}}|} \tag{A.17b}$$

where

$$\widehat{\boldsymbol{R}}_{yy} = \frac{1}{NK}\sum_{k=1}^{K}(\boldsymbol{Y}_{\mathrm{T},k}\boldsymbol{Y}_{\mathrm{T},k}^{H} + \boldsymbol{Z}_k\boldsymbol{Z}_k^{H}) \text{ and} \tag{A.18a}$$

$$\overline{\boldsymbol{Y}}_{\mathrm{T}} = \frac{1}{K}\sum_{k=1}^{K}\boldsymbol{Y}_{\mathrm{T},k}. \tag{A.18b}$$

We may also rearrange the above test statistic in the form of

$$\mathrm{GLR} = |\boldsymbol{I}_d + \boldsymbol{V}^H\boldsymbol{T}^{-1}\boldsymbol{V}| \tag{A.19a}$$

$$= \frac{|\boldsymbol{T} + \boldsymbol{V}\boldsymbol{V}^H|}{|\boldsymbol{T}|} \tag{A.19b}$$

where

$$\boldsymbol{T} = (\boldsymbol{Y} - \overline{\boldsymbol{Y}}_{\mathrm{T}}\boldsymbol{\Phi})(\boldsymbol{Y} - \overline{\boldsymbol{Y}}_{\mathrm{T}}\boldsymbol{\Phi})^H \text{ and} \tag{A.20a}$$

$$\boldsymbol{V} = \frac{1}{\sqrt{N}}\overline{\boldsymbol{Y}}_{\mathrm{T}}. \tag{A.20b}$$

As in the real data case, $\boldsymbol{T}$ can be expressed in terms of complex Gaussian array $\boldsymbol{W}$ of dimension $j \times NK + j - m - d$ as follows:

$$\boldsymbol{T} = \boldsymbol{W}\boldsymbol{W}^H. \tag{A.21}$$

APPENDIX B. EXPLICIT FORM OF GLR TEST

In this appendix, we demonstrate the derivation of the explicit form of the GLR test for both real and complex data scenarios.

Real Data Scenario

For the real case in Appendix A, the GLR test statistic is derived as follows:

$$\begin{aligned} \text{GLR} &= |\boldsymbol{I}_d + \boldsymbol{V}^T \boldsymbol{T}^{-1} \boldsymbol{V}| && \text{(B.1a)} \\ &= \frac{|\boldsymbol{T} + \boldsymbol{V}\boldsymbol{V}^T|}{|\boldsymbol{T}|} && \text{(B.1b)} \end{aligned}$$

where $\boldsymbol{T} = \boldsymbol{W}\boldsymbol{W}^T$. The arrays $\boldsymbol{V}$ of size $j \times d$ and $\boldsymbol{W}$ of size $j \times NK + j - m - d$ are zero-mean Gaussian and independent of one another. Here, we introduce a new quantity $\widetilde{K} = NK - m - d$ and recall that $\widetilde{K} \geq 0$. From (B.1a), we define the term inside the determinant $|\cdot|$ by the following function:

$$\mathcal{L}(j, d, \widetilde{K}) = \boldsymbol{I}_d + \boldsymbol{V}^T \boldsymbol{T}^{-1} \boldsymbol{V}. \qquad \text{(B.2)}$$

The arrays $\boldsymbol{V}$ and $\boldsymbol{W}$ can be partitioned into

$$\begin{aligned} \boldsymbol{V} &= \begin{bmatrix} \boldsymbol{V}_1 \\ \boldsymbol{V}_2 \end{bmatrix} && \text{(B.3a)} \\ \boldsymbol{W} &= \begin{bmatrix} \boldsymbol{W}_1 \\ \boldsymbol{W}_2 \end{bmatrix} && \text{(B.3b)} \end{aligned}$$

where $\boldsymbol{V}_1$, $\boldsymbol{V}_2$, $\boldsymbol{W}_1$, and $\boldsymbol{W}_2$ are matrices having the size of $j_1 \times d$, $j_2 \times d$, $j_1 \times \widetilde{K} + j$, and $j_2 \times \widetilde{K} + j$, respectively. The matrix $\boldsymbol{T}$ can be represented by

$$\boldsymbol{T} = \begin{bmatrix} \boldsymbol{W}_1\boldsymbol{W}_1^T & \boldsymbol{W}_1\boldsymbol{W}_2^T \\ \boldsymbol{W}_2\boldsymbol{W}_1^T & \boldsymbol{W}_2\boldsymbol{W}_2^T \end{bmatrix} \tag{B.4a}$$

$$= \begin{bmatrix} \boldsymbol{T}_{11} & \boldsymbol{T}_{12} \\ \boldsymbol{T}_{21} & \boldsymbol{T}_{22} \end{bmatrix}. \tag{B.4b}$$

We also define

$$\boldsymbol{T}^{-1} = \begin{bmatrix} \boldsymbol{T}^{11} & \boldsymbol{T}^{12} \\ \boldsymbol{T}^{21} & \boldsymbol{T}^{22} \end{bmatrix} \tag{B.5}$$

and then substitute:

$$\boldsymbol{V}^H\boldsymbol{T}^{-1}\boldsymbol{V} = \begin{bmatrix} \boldsymbol{V}_1^T & \boldsymbol{V}_2^T \end{bmatrix} \begin{bmatrix} \boldsymbol{T}^{11} & \boldsymbol{T}^{12} \\ \boldsymbol{T}^{21} & \boldsymbol{T}^{22} \end{bmatrix} \begin{bmatrix} \boldsymbol{V}_1 \\ \boldsymbol{V}_2 \end{bmatrix} \tag{B.6a}$$

$$= \boldsymbol{V}_1^T\boldsymbol{T}^{11}\boldsymbol{V}_1 + \boldsymbol{V}_2^T\boldsymbol{T}^{21}\boldsymbol{V}_1 + \boldsymbol{V}_1^T\boldsymbol{T}^{12}\boldsymbol{V}_2 + \boldsymbol{V}_2^T\boldsymbol{T}^{22}\boldsymbol{V}_2. \tag{B.6b}$$

The above equation can be rearranged in the form of

$$\begin{aligned} \boldsymbol{V}^T\boldsymbol{T}^{-1}\boldsymbol{V} &= \boldsymbol{V}_1^T\boldsymbol{T}^{11}\boldsymbol{V}_1 + \boldsymbol{V}_2^T\boldsymbol{T}^{21}\boldsymbol{T}^{11}(\boldsymbol{T}^{11})^{-1}\boldsymbol{V}_1 + \boldsymbol{V}_1^T\boldsymbol{T}^{11}(\boldsymbol{T}^{11})^{-1}\boldsymbol{T}^{12}\boldsymbol{V}_2 + \\ &\quad \boldsymbol{V}_2^T\boldsymbol{T}^{22}\boldsymbol{V}_2 + \boldsymbol{V}_2^T\boldsymbol{T}^{21}(\boldsymbol{T}^{11})^{-1}\boldsymbol{T}^{11}(\boldsymbol{T}^{11})^{-1}\boldsymbol{T}^{12}\boldsymbol{V}_2 - \\ &\quad \boldsymbol{V}_2^T\boldsymbol{T}^{21}(\boldsymbol{T}^{11})^{-1}\boldsymbol{T}^{11}(\boldsymbol{T}^{11})^{-1}\boldsymbol{T}^{12}\boldsymbol{V}_2 \qquad \text{(B.7a)} \\ &= (\boldsymbol{V}_1^T + \boldsymbol{V}_2^T\boldsymbol{T}^{21}(\boldsymbol{T}^{11})^{-1})\,\boldsymbol{T}^{11}\,(\boldsymbol{V}_1 + (\boldsymbol{T}^{11})^{-1}\boldsymbol{T}^{12}\boldsymbol{V}_2) + \\ &\quad \boldsymbol{V}_2^T(\boldsymbol{T}^{22} - \boldsymbol{T}^{21}(\boldsymbol{T}^{11})^{-1}\boldsymbol{T}^{12})\boldsymbol{V}_2. \qquad \text{(B.7b)} \end{aligned}$$

In order to simplify the equation above, we may use the following identity of matrix inversion. For any non-singular matrix M that can be partitioned into

$$M = \begin{bmatrix} A & B \\ C & D \end{bmatrix} \tag{B.7a}$$

where A and D are square and non-singular matrices, the inverse version of the matrix M can be presented in the form of

$$M^{-1} = \begin{bmatrix} A^{-1} + A^{-1}B(D - CA^{-1}B)^{-1}CA^{-1} & -A^{-1}B(D - CA^{-1}B)^{-1} \\ -(D - CA^{-1}B)^{-1}CA^{-1} & (D - CA^{-1}B)^{-1} \end{bmatrix} \tag{B.8a}$$

$$= \begin{bmatrix} (A - BD^{-1}C)^{-1} & -(A - BD^{-1}C)^{-1}BD^{-1} \\ -D^{-1}C(A - BD^{-1}C)^{-1} & D^{-1} + D^{-1}C(A - BD^{-1}C)^{-1}BD^{-1} \end{bmatrix} \tag{B.8b}$$

By applying the identity above, we obtain

$$V^T T^{-1} V = (V_1 + T_{12}T_{22}^{-1}V_2)^T T^{11} (V_1 + T_{12}T_{22}^{-1}V_2) + V_2^T T_{22}^{-1} V_2 \tag{B.9}$$

and by adding the identity matrix I_d, we may express (B.2) in the form of products:

$$\mathcal{L}(j, d, \widetilde{K}) = (I_d + V_2^T T_{22}^{-1} V_2)^{1/2} (I_d + \mathcal{V}^T \mathcal{T}^{-1} \mathcal{V}^T)(I_d + V_2^T T_{22}^{-1} V_2)^{1/2} \tag{B.10}$$

where

$$\mathcal{V} = (V_1 - T_{12}T_{22}^{-1}V_2{}^T)(I_d + V_2^T T_{22}^{-1} V_2)^{-1/2}, \text{ and} \tag{B.11a}$$

$$\mathcal{T} = (T^{11})^{-1} = T_{11} - T_{12}T_{22}^{-1}T_{21}. \tag{B.11b}$$

Clearly, $\boldsymbol{V}_2$ and $\boldsymbol{W}_2$ are zero-mean Gaussian and independent of one another. We may represent the first and last terms of (B.10) by

$$\boldsymbol{I}_d + \boldsymbol{V}_2^T \boldsymbol{T}_{22}^{-1} \boldsymbol{V}_2 = \mathcal{L}(j_2, d, j_1 + \widetilde{K}). \tag{B.12}$$

The matrix $\boldsymbol{\mathcal{V}}$ of size $j_1 \times d$ is zero-mean Gaussian and independent from $\boldsymbol{\mathcal{T}}$. Since $\boldsymbol{\mathcal{T}}$ is a Wishart matrix of dimension j_1 and with $j_1 + \widetilde{K}$ degrees of freedom, we may express $\boldsymbol{\mathcal{T}}$ in the form of

$$\boldsymbol{\mathcal{T}} = \widetilde{\boldsymbol{\mathcal{W}}} \widetilde{\boldsymbol{\mathcal{W}}}^H \tag{B.13}$$

where $\widetilde{\boldsymbol{\mathcal{W}}}$ is a zero-mean Gaussian array with the size of $j_1 \times j_1 + \widetilde{K}$. Thus, the middle term of (B.10) can be presented by the following equation:

$$\boldsymbol{I}_d + \boldsymbol{\mathcal{V}}^T \boldsymbol{\mathcal{T}}^{-1} \boldsymbol{\mathcal{V}}^T = \mathcal{L}(j_1, d, \widetilde{K}). \tag{B.14}$$

From the results above, we may conclude that

$$\begin{aligned} \text{GLR} &= |\mathcal{L}(j, d, \widetilde{K})| && \text{(B.15a)} \\ &= |\mathcal{L}(j - j_1, d, j_1 + \widetilde{K})| \, |\mathcal{L}(j_1, d, \widetilde{K})| && \text{(B.15b)} \\ &= \prod_{i=0}^{j-1} |\mathcal{L}(1, d, \widetilde{K} + i)|. && \text{(B.15c)} \end{aligned}$$

Now, we consider a special case for $|\mathcal{L}(j,d,\widetilde{K})|$ when $j=1$, i.e. $\boldsymbol{W}$ is a row vector. We may represent

$$\boldsymbol{T} = \boldsymbol{W}\boldsymbol{W}^T = \sum_{i=1}^{\widetilde{K}} w_i^2, \tag{B.16a}$$

$$\boldsymbol{V}\boldsymbol{V}^T = \sum_{k=1}^{d} v_k^2, \text{ and} \tag{B.16b}$$

$$|\mathcal{L}(j,d,\widetilde{K})| = \frac{\sum_{i=1}^{\widetilde{K}} w_i^2 + \sum_{k=1}^{d} v_k^2}{\sum_{i=1}^{\widetilde{K}} w_i^2} \tag{B.16c}$$

where w_i and v_k in this case are the elements of row vectors $\boldsymbol{W}$ and $\boldsymbol{V}$, respectively. Since w_i and v_k are zero-mean Gaussian and independent of one another, $\sum_{i=1}^{\widetilde{K}} w_i^2$ and $\sum_{k=1}^{d} v_k^2$ are χ^2 random variables with $\widetilde{K}$ and d degrees of freedom, respectively and

$$\frac{1}{|\mathcal{L}(1,d,\widetilde{K})|} = \frac{\sum_{i=1}^{\widetilde{K}} w_i^2}{\sum_{i=1}^{\widetilde{K}} w_i^2 + \sum_{k=1}^{d} v_k^2} \tag{B.17a}$$

$$\equiv x_\beta\Big(\frac{\widetilde{K}}{2}, \frac{d}{2}\Big) \tag{B.17b}$$

where $x_\beta(n,m)$ denotes a beta random variable with parameter n and m. By substituting the result from (B.17b) into (B.15c), we obtain the product of independent beta random variables as follows:

$$\frac{1}{\text{GLR}} = \prod_{i=1}^{j} x_\beta^{(i)}\Big(\frac{\widetilde{K}+i}{2}, \frac{d}{2}\Big) \tag{B.18a}$$

$$= \prod_{i=1}^{m} x_\beta^{(i)}\Big(\frac{NK-d-m+i}{2}, \frac{d}{2}\Big) \tag{B.18b}$$

$$\sim \lambda(m, NK-d, d) \tag{B.18c}$$

where $\lambda(m,n,p)$ denotes Wilks' lambda distribution with parameter m, n, and p. Recall that $\widetilde{K} = NK-m-d$ and for the model in Chapter 2, $j=m$. Obviously, when $j=1$, 1/GLR is a single beta variable with parameters $NK-d-m+1$ and d.

Complex Data Scenario

For the complex data scenario, by applying the same method as in the real case, 1/GLR can be represented by the product of independent beta random variables as follows:

$$\frac{1}{\text{GLR}} = \prod_{i=1}^{j} x_{\beta}^{(i)}(\widetilde{K}+i,d) \tag{B.19a}$$

$$= \prod_{i=1}^{m} x_{\beta}^{(i)}(NK-d-m+i,d) \tag{B.19b}$$

$$\sim \lambda_C(m,NK-d,d) \tag{B.19c}$$

where $\lambda_C(m,n,p)$ denotes complex Wilks' lambda distribution with parameter m, n, and p.

APPENDIX C. NUMERICAL EXPRESSION OF GLR TEST DISTRIBUTIONS

In Appendix B, even though we obtained the explicit form of the GLR test, there is still a problem of computing the exact distribution of the test when j is greater than 1, i.e. 1/GLR is not a single beta random variable. In this appendix, we show the derivation of numerical expression for computing the exact probability density function and determining decision thresholds for a specified probability of false alarms P_{FA}.

Real Data Scenario

For a real data scenario, in order to determine the numerical expression, we first consider a special case of an expected value of a beta random variable x_β with parameters $(\widetilde{m}, \widetilde{n})$. The PDF of x_β is given by

$$f_\beta(x; \widetilde{m}, \widetilde{n}) = \frac{1}{B(\widetilde{m}, \widetilde{n})} x^{\widetilde{m}-1}(1-x)^{\widetilde{n}-1} \tag{C.1}$$

where $0 \leq x \leq 1, \widetilde{m} > 0$, and $\widetilde{n} > 0$. Here, $B(\widetilde{m}, \widetilde{n})$ represents $\frac{\Gamma(\widetilde{m})\Gamma(\widetilde{n})}{\Gamma(\widetilde{m}+\widetilde{n})}$ and $\Gamma(n)$ denotes a gamma function with a parameter n. For any positive value k, the expected value of x_β^k is described below:

$$\begin{aligned} \mathrm{E}[x_\beta^k] &= \int_0^1 x^k f_\beta(x; \widetilde{m}, \widetilde{n}) dx & \text{(C.2a)} \\ &= \frac{\Gamma(\widetilde{m}+\widetilde{n})\,\Gamma(k+\widetilde{m})}{\Gamma(k+\widetilde{m}+\widetilde{n})\,\Gamma(\widetilde{m})}. & \text{(C.2b)} \end{aligned}$$

From the result in Appendix B, a Wilks' lambda random variable can be represented in the form of the product of beta random variables. Thus, by applying the result in (C.2b) to a Wilks' lambda random variable λ with parameters $(m, NK-d, d)$, we obtain

$$\mathrm{E}[\lambda^k] = \int_0^1 x^k f_\lambda(\lambda; m, NK-d, d)dx \tag{C.3a}$$

$$= \prod_{i=1}^{m} \frac{\Gamma(\frac{NK-m+i}{2})\,\Gamma(\frac{NK-m-d+i}{2}+k)}{\Gamma(\frac{NK-m-d+i}{2})\,\Gamma(\frac{NK-m+i}{2}+k)} \tag{C.3b}$$

where $f_\lambda(\lambda; m, n, p)$ denotes the PDF of λ with parameters m, n, and p. By utilizing the method in [23] with the obtained result in (C.3b), the PDF of λ, or 1/GLR in this case, can be computed using the following equation:

$$f_\lambda(\lambda; m, NK-d, d) = \Big[\prod_{j=1}^{m} \frac{\Gamma(\frac{NK-m+j}{2})}{\Gamma(\frac{NK-m-d+j}{2})}\Big]\lambda^{\mu-1} \sum_{r=0}^{\infty} \frac{l_r}{\Gamma(r+md/2)}(-\ln\lambda)^{r+\frac{md}{2}-1} \tag{C.4}$$

where μ is a constant chosen to satisfy $0 \le \mu < (NK-m-d+1)/2$; $l_0 = 1$, $l_r = \sum_{k=1}^{r} k\, q_k\, l_{r-k}$, and

$$q_k = (-1)^{k+1}[k(k+1)]^{-1}\Big\{\sum_{j=1}^{m} B_{k+1}\Big(\frac{NK-m-d+j}{2}-\mu\Big) - \sum_{j=1}^{m} B_{k+1}\Big(\frac{NK-m+j}{2}-\mu\Big)\Big\},\quad k=1,2,\ldots,$$

where $B_r(\cdot)$ denotes the Bernoulli polynomial of degree r. The probability of false alarms can be determined from

$$\begin{aligned} P_{\text{FA}} &= P(\text{GLR} > \tau) && \text{(C.5a)} \\ &= P(\lambda < 1/\tau) = 1 - P(\lambda > 1/\tau) && \text{(C.5b)} \\ &= 1 - \int_{1/\tau}^{1} f_\lambda(\lambda) d\lambda && \text{(C.5c)} \\ &= 1 - \Big[\prod_{j=1}^{m} \frac{\Gamma(\frac{NK-m+j}{2})}{\Gamma(\frac{NK-m-d+j}{2})}\Big] \sum_{r=0}^{\infty} \frac{l_r}{\mu^{(r+md/2)}} \Gamma_{\text{inc}}\Big(\mu \ln \tau,\ r + \frac{md}{2}\Big) && \text{(C.5d)} \end{aligned}$$

where $\Gamma_{\text{inc}}(x, a)$ is the incomplete gamma function at value x with parameter a. The GLR threshold τ for a specified P_{FA} can be determined by solving (C.5d).

Complex Data Scenario

For a complex data scenario, by applying the same method as in the real case, we obtain an equation for the expected value of a complex Wilks' lambda random variable λ with parameters $(m, NK - d, d)$ as follows:

$$\begin{aligned} \text{E}[\lambda^k] &= \int_0^1 x^k f_{\lambda_C}(\lambda; m, NK-d, d) dx && \text{(C.6a)} \\ &= \prod_{i=1}^{m} \frac{\Gamma(NK-m+i)\,\Gamma(NK-m-d+i+k)}{\Gamma(NK-m-d+i)\,\Gamma(NK-m+i+k)} && \text{(C.6b)} \end{aligned}$$

where $f_{\lambda_C}(\lambda; m, n, p)$ denotes the PDF of λ with parameters m, n, and p. Thus, the PDF of λ (or 1/GLR) can be computed using the following equation:

$$f_{\lambda_C}(\lambda; m, NK-d, d) = \Big[\prod_{j=1}^{m} \frac{\Gamma(NK-m+j)}{\Gamma(NK-m-d+j)}\Big] \lambda^{\mu-1} \sum_{r=0}^{\infty} \frac{l_r}{\Gamma(r+md)} (-\ln \lambda)^{r+md-1} \qquad \text{(C.7)}$$

where μ is a constant chosen to satisfy $0 \leq \mu < (NK-m-d+1)$; $l_0 = 1$, $l_r = \sum_{k=1}^{r} k q_k l_{r-k}$, and

$$q_k = (-1)^{k+1}[k(k+1)]^{-1}\Big\{\sum_{j=1}^{m} B_{k+1}(NK-m-d+j-\mu) - \sum_{j=1}^{m} B_{k+1}(NK-m+j-\mu)\Big\}, \quad k = 1, 2, \ldots.$$

The probability of false alarms can be determined from

$$P_{\text{FA}} = P(\text{GLR} > \tau) \tag{C.8a}$$

$$= P(\lambda < 1/\tau) = 1 - P(\lambda > 1/\tau) \tag{C.8b}$$

$$= 1 - \int_{1/\tau}^{1} f_{\lambda_C}(\lambda) d\lambda \tag{C.8c}$$

$$= 1 - \Big[\prod_{j=1}^{m} \frac{\Gamma(NK-m+j)}{\Gamma(NK-m+j)}\Big] \sum_{r=0}^{\infty} \frac{l_r}{\mu^{(r+md)}} \Gamma_{\text{inc}}(\mu \log \tau,\ r+md) \tag{C.8d}$$

where the GLR threshold τ for a specified P_{FA} can be determined by solving (C.8d).

APPENDIX D. SPECIAL CASE FOR GLR TEST

Problem Formulation and Test Statistic

In Appendix A, the GLR test for a general model has been derived for detecting the presence of the defect signal $\boldsymbol{X}$. In that case, the elements of $\boldsymbol{X}$ can be either positive or negative. In this appendix, we consider the GLR test under a real data scenario for a special case when all elements of $\boldsymbol{X}$ are positive. Hence, the detection problem becomes: testing null hypothesis

$$\mathcal{H}_0 : \boldsymbol{X} = \boldsymbol{0}$$

versus the alternative

$$\mathcal{H}_1 : \boldsymbol{X} \succeq \boldsymbol{0}$$

where $\boldsymbol{X} \succeq 0$ denotes that all elements of $\boldsymbol{X}$ are greater than or equal to zero. We use the same model and configuration as in (A.1) and (A.9), respectively. By utilizing the ML estimators in (A.4), the test statistic for the above model is given by

$$\text{Test statistic} \equiv \frac{|\widehat{\boldsymbol{\Sigma}}_0|}{\min\limits_{\boldsymbol{X}\succeq\boldsymbol{0}} |\widehat{\boldsymbol{\Sigma}}_1|} \tag{D.1a}$$

$$= \frac{|\widehat{\boldsymbol{R}}_{yy}|}{\min\limits_{\boldsymbol{X}\succeq\boldsymbol{0}} \left|(1/N)\cdot\sum_{k=1}^{K}[\boldsymbol{Z}_k\boldsymbol{Z}_k^T + (\boldsymbol{Y}_{T,k}-\boldsymbol{X})(\boldsymbol{Y}_{T,k}-\boldsymbol{X})^T]\right|}. \tag{D.1b}$$

Recall that $\widehat{\boldsymbol{R}}_{yy} = \widehat{\boldsymbol{\Sigma}}_0 = \sum_{k=1}^{K}(\boldsymbol{Z}_k\boldsymbol{Z}_k^T + \boldsymbol{Y}_{\mathrm{T},k}\boldsymbol{Y}_{\mathrm{T},k}^T)$. The denumerator in (D.1b) can be rearranged in the form of

$$|\,(1/N)\cdot\boldsymbol{\mathcal{Z}}\boldsymbol{\mathcal{Z}}^T|\cdot|\boldsymbol{I}_m + (\boldsymbol{\mathcal{Z}}\boldsymbol{\mathcal{Z}}^T)^{-1}(\boldsymbol{\mathcal{Y}}_{\mathrm{T}} - \boldsymbol{X}\widetilde{\boldsymbol{\Phi}})(\boldsymbol{\mathcal{Y}}_{\mathrm{T}} - \boldsymbol{X}\widetilde{\boldsymbol{\Phi}})^T| \tag{D.2}$$

where

$$\boldsymbol{\mathcal{Z}} = [\boldsymbol{Z}_1 \ \ldots \ \boldsymbol{Z}_K]_{m\times(N-d)K}, \tag{D.3a}$$

$$\boldsymbol{\mathcal{Y}}_T = [\boldsymbol{Y}_{\mathrm{T},1} \ \ldots \ \boldsymbol{Y}_{\mathrm{T},K}]_{m\times dK}, \text{ and} \tag{D.3b}$$

$$\widetilde{\boldsymbol{\Phi}} = [\boldsymbol{I}_d \ \ldots \ \boldsymbol{I}_d]_{d\times dK}. \tag{D.3c}$$

Now we consider Taylor series expansion for $|\boldsymbol{I}+\boldsymbol{A}|$ where $\boldsymbol{I}$ is an identity matrix and $\boldsymbol{A}$ is an arbitrary matrix with the the same size as $\boldsymbol{I}$. The Taylor series expansion is expressed as

$$\ln|\boldsymbol{I}+\boldsymbol{A}| \approx \mathrm{Tr}(\boldsymbol{A}) + (1/2)\cdot\mathrm{Tr}(\boldsymbol{A}^2) + \ldots \tag{D.4}$$

and

$$\ln|\boldsymbol{I}+\boldsymbol{A}| \approx \mathrm{Tr}(\boldsymbol{A}). \tag{D.5}$$

for a small $\boldsymbol{A}$. Let $L = |\boldsymbol{I}_m + (\boldsymbol{\mathcal{Z}}\boldsymbol{\mathcal{Z}}^T)^{-1}(\boldsymbol{\mathcal{Y}}_{\mathrm{T}} - \boldsymbol{X}\widetilde{\boldsymbol{\Phi}})(\boldsymbol{\mathcal{Y}}_{\mathrm{T}} - \boldsymbol{X}\widetilde{\boldsymbol{\Phi}})^T|$. Assuming that $\boldsymbol{\mathcal{Z}}$ has a large number of columns, we may simplify the problem under this scenario by applying the above approximation as follows:

$$\ln L \approx \mathrm{Tr}[(\boldsymbol{\mathcal{Z}}\boldsymbol{\mathcal{Z}}^T)^{-1}(\boldsymbol{\mathcal{Y}}_{\mathrm{T}} - \boldsymbol{X}\widetilde{\boldsymbol{\Phi}})(\boldsymbol{\mathcal{Y}}_{\mathrm{T}} - \boldsymbol{X}\widetilde{\boldsymbol{\Phi}})^T]. \tag{D.6}$$

Hence, minimizing $|\widehat{\Sigma}_1|$ subject to $\boldsymbol{X} \succeq \mathbf{0}$ is approximately equivalent to

$$\min_{\boldsymbol{X}\succeq\mathbf{0}} |\widehat{\Sigma}_1| \;\cong\; \min_{\boldsymbol{X}\succeq\mathbf{0}} \mathrm{Tr}[(\boldsymbol{Z}\boldsymbol{Z}^T)^{-1}(\boldsymbol{\mathcal{Y}}_{\mathrm{T}} - \boldsymbol{X}\Phi)(\boldsymbol{\mathcal{Y}}_{\mathrm{T}} - \boldsymbol{X}\Phi)^T] \tag{D.7a}$$

$$= \sum_{k=1}^{K}\sum_{i=1}^{d} \min_{\boldsymbol{x}_i\succeq\mathbf{0}} (\boldsymbol{y}_{\mathrm{T},k,i} - \boldsymbol{x}_i)^T(\boldsymbol{Z}\boldsymbol{Z}^T)^{-1}(\boldsymbol{y}_{\mathrm{T},k,i} - \boldsymbol{x}_i) \tag{D.7b}$$

where $[\boldsymbol{y}_{\mathrm{T},k,1}\ \boldsymbol{y}_{\mathrm{T},k,2}\ \cdots\ \boldsymbol{y}_{\mathrm{T},k,d}]$ and $[\boldsymbol{x}_1\ \boldsymbol{x}_2\ \ldots\ \boldsymbol{x}_d]$ are column vectors of $\boldsymbol{Y}_{\mathrm{T},k}$ and $\boldsymbol{X}$, respectively. By utilizing the method in [24, Ch. 4.2], the optimality conditions for minimizing the above equation subject to $\boldsymbol{x}_i \succeq \mathbf{0}$ can be expressed as

$$\boldsymbol{x}_i \;\succeq\; \mathbf{0}, \tag{D.8a}$$

$$-(\boldsymbol{Z}\boldsymbol{Z}^T)^{-1}(\overline{\boldsymbol{y}}_{\mathrm{T},i} - \boldsymbol{x}_i) \;\succeq\; \mathbf{0}, \text{ and} \tag{D.8b}$$

$$x_{i,j}[(\boldsymbol{Z}\boldsymbol{Z}^T)^{-1}(\overline{\boldsymbol{y}}_{\mathrm{T},i} - \boldsymbol{x}_i)]_j \;=\; 0,\ \ j = 1, 2, \ldots, m, \tag{D.8c}$$

where $\overline{\boldsymbol{y}}_{\mathrm{T},i} = (1/K)\cdot\sum_{k=1}^{K}\boldsymbol{y}_{\mathrm{T},k,i}$ and $x_{i,j}$ denote the elements of $\boldsymbol{x}_i$. The GLR test can be obtained by substituting the estimator of $\boldsymbol{X}$, denoted by $\widehat{\boldsymbol{X}}$, that satisfies the optimality conditions in (D.8) into (D.1b) as follows:

$$\mathrm{GLR} = \frac{|\widehat{\boldsymbol{R}}_{yy}|}{\left|(1/N)\cdot\sum_{k=1}^{K}[\boldsymbol{Z}_k\boldsymbol{Z}_k^T + (\boldsymbol{Y}_{\mathrm{T},k} - \widehat{\boldsymbol{X}})(\boldsymbol{Y}_{\mathrm{T},k} - \widehat{\boldsymbol{X}})^T]\right|}. \tag{D.9}$$

For the energy detector, the test under this scenario is given by

$$\mathrm{ED} = \frac{N-d}{d}\cdot\frac{\mathrm{Tr}(\overline{\boldsymbol{Y}}_{\mathrm{T}}\overline{\boldsymbol{Y}}_{\mathrm{T}}^{\mathrm{T}})}{\mathrm{Tr}[\overline{\boldsymbol{Z}}\overline{\boldsymbol{Z}}^{\mathrm{T}} + (\overline{\boldsymbol{Y}}_{\mathrm{T}} - \widehat{\boldsymbol{X}})(\overline{\boldsymbol{Y}}_{\mathrm{T}} - \widehat{\boldsymbol{X}})^{\mathrm{T}}]} \tag{D.10}$$

where the ML estimator $\widehat{\boldsymbol{X}}$ in this case, is obtained by replacing the negative elements of $\overline{\boldsymbol{Y}}_{\mathrm{T}}$ with zero.

Newton-Raphson Method

In practise, it is not convenient to find the estimator of $\boldsymbol{X}$ for the GLR test that satisfies the optimality conditions in (D.8). By applying the method in [24, Ch. 11.8] and Newton-Raphson algorithm, we obtain an iteration for computing the approximate estimator of $\boldsymbol{x}_i$ as follows:

$$\boldsymbol{x}_i^{\text{new}} = \boldsymbol{x}_i^{\text{old}} - \mu \boldsymbol{H}^{-1}\boldsymbol{g} \tag{D.11}$$

where $\boldsymbol{x}_i^{\text{new}}$ is an updated $\boldsymbol{x}_i$ and $\boldsymbol{x}_i^{\text{old}}$ is $\boldsymbol{x}_i$ in the previous step. Here, μ is a constant chosen between 0 and 1. The matrix $\boldsymbol{H}$ and vector $\boldsymbol{g}$ are determined using the following equations:

$$\boldsymbol{H} = t\,[2(\boldsymbol{Z}\boldsymbol{Z}^T)^{-1}] + \boldsymbol{\mathcal{A}}, \text{ and} \tag{D.12a}$$

$$\boldsymbol{g} = -t\,[2(\boldsymbol{Z}\boldsymbol{Z}^T)^{-1}(\overline{\boldsymbol{y}}_{\mathrm{T},i} - \boldsymbol{x}_i^{\text{old}})] - \boldsymbol{b}. \tag{D.12b}$$

where t is a positive constant, $\boldsymbol{b} = [1/x_{i,1} \ \ldots \ 1/x_{i,m}]^T$, and

$$\boldsymbol{\mathcal{A}} = \begin{bmatrix} \frac{1}{x_{i,1}^2} & 0 & 0 & \ldots & 0 \\ 0 & \frac{1}{x_{i,2}^2} & 0 & \ldots & 0 \\ 0 & 0 & \frac{1}{x_{i,3}^2} & \ldots & 0 \\ \vdots & \vdots & \vdots & \ddots & \vdots \\ 0 & 0 & 0 & \ldots & \frac{1}{x_{i,m}^2} \end{bmatrix}.$$

The iteration is terminated when $\boldsymbol{x}_i^{\text{new}}$ and $\boldsymbol{x}_i^{\text{old}}$ are not much different. When t is large, the approximate estimator of $\boldsymbol{x}_i$ approaches the true estimator that maximizes the GLR test.

BIBLIOGRAPHY

[1] Auld, B. A. and Moulder, J. C. (1999). *J. Nondestructive Eval.*, *18*, 3–36.

[2] Thompson, R. B. and Thompson, D. O. (1985). Ultrasonic in NDE Evaliation. *Proceeding of the IEEE*, *73*(12), 1716–1755.

[3] Dinten, J. M., Dziopa, P., and Koenig, A. (1994). X-rays image analysis for defects detection and characterization in metallic samples. *Image Processing, Proceedings. ICIP-94., IEEE International Conference*, *2*, 321–325

[4] Casella, G. and Berger, R. L. (2001). *Statistical Inference Second Edition.* Pacific Groove, CA: Duxbury Press.

[5] Thompson, R. B. and Gray, T. A. (1986). *Phil. Trans. R. Soc. Lond.*, *320*, 329–340.

[6] Dogandžić, A. and Nehorai, A. (2003). *IEEE Signal Processing Magazine*, *20*, 39–54.

[7] Kay, S. M. (1998). *Fundamentals of Statistical Signal Processing: Detection Theory.* Englewood Cliffs, NJ: Prentice Hall, pt. II.

[8] Dogandžić, A. and Nehorai, A. (2000). *IEEE Trans. Signal Processing*, *48*, 13–25.

[9] Dogandžić, A. and Nehorai, A. (2003). EEG/MEG spatio-temporal dipole source estimation and array design. *High-Resolution and Robust Signal Processing.* A.B. Gershman and Y. Hua, Eds., New York: Marcel Dekker, 393–442.

[10] Srivastava, M. S. and Carter, E. M. (1983). *An Introduction to Applied Multivariate Statistics.* New York, North-Holland.

[11] Kalos, M. H. and Whitelock, P. A. (1986). *Monte Carlo Methods.* New York: John Wiley and Sons.

[12] Madras, N. (1998). *Monte Carlo Methods.* Rhode Island: American Mathematical Society.

[13] Zwillinger, D. (1986). *Standard Mathematical Tables and Formulae Thirtieth Edition.* Boca Raton, FL: CRC Press.

[14] Kelly, E. J. and Forsythe, K. M. (1989). "Adaptive detection and parameter estimation for multidimensional signal models." Lincoln Lab., Mass. Inst. Technol., Lexington, MA, Tech. Rep. 848.

[15] Howard, P. J., Copley, D. C., and Gilmore, R. S. (1998). The application of a dynamic threshold to C-scan images with variable noise. *Review of Progress in Quantitative Nondestructive Evaluation, 17,* 2013–2019.

[16] Willsky, A. S. (2002). "Multiresolution Markov models for signal and image processing," *Proc. IEEE, 90,* 1396–1458.

[17] Ephraim, Y. and Merhav, N. (2002). "Hidden Markov processes," *IEEE Trans. Inform. Theory, 47,* 1518–1569.

[18] Besag, J. (1974). "Spatial interaction and statistical-analysis of lattice systems," *J. R. Stat. Soc., Ser. B, 36,* 192–236.

[19] Cressie, N. A. C. (1993). *Statistics for Spatial Data.* revised ed., New York: Wiley.

[20] Besag, J. (1986). "On the statistical analysis of dirty pictures." *J. R. Stat. Soc., Ser. B, 48,* 259–302.

[21] Ripley, B. D. (1988). *Statistical Inference for Spatial Processes.* Cambridge, UK: Cambridge Univ. Press.

[22] MacKay, D. J. (2003). *Information Theory, Inference, and Learning Algorithms.* Cambridge, UK: Cambridge University Press

[23] Tang, J. and Gupta, A. K. (1986). Exact Distribution of Certain General Test Statistics in Multivariate Analysis, *Austral. J. Statist.*, *28*(1), 107–114

[24] Boyd, S. and Vandenberghe, L. (2002). *Convex Optimization.*

ACKNOWLEDGEMENTS

I would like to take this opportunity to thank many people who have helped and supported me towards the completion of my Master's degree. First and foremost, I would like to express my sincere gratitude to my major professor, Dr. Aleksandar Dogandžić, for his guidance, patience, and friendship throughout my graduate study. His insights and words of encouragement have often inspired and encouraged me to overcome all difficulties. I am deeply indebted to him for his tireless support and devotion.

I would also sincerely thank my committees, Dr. Joseph N. Gray and Dr. Zhengdao Wang for their kindly suggestions, efforts, and contributions to this work.

Additionally, I would give special thanks to the National Science Foundation (NSF) Industry-University Cooperative Research Program, Center for Nondestructive Evaluation (CNDE), Iowa State University for research financial support. I am also grateful to Dr. Bruce Thompson from CNDE and Dr. Waled Hassan from Honeywell International Inc. for the experimental data and excellent advices.

I deeply appreciate the Electricity Generating Authority of Thailand (EGAT) for providing me a great opportunity to study here. I would also give my appreciation to all of my colleagues at EGAT, especially, Gunchat Sangmanee, Nuchan Namonta, Pasara Tovichakchaikul, Nanthana Yutithum, and Luckana Kakaew for their kindly support and encouragement.

Furthermore, I would like to thank all of my instructors and friends, especially, Dr. Volker H. Hegelheimer, Jenifer L. Thornburg, Dr. Dennis Wendell, Prasit Boonma, Supapan Sangnui, Sonthaya Tiawsirisup, Worapa Anothayanon, Somjai Kidrungruang, Pariya Wattanadamrongrat, Ladda Pitaksringkarn, Varaporn Sangtong, Yuwadee Ungsriwong, Pipat Reungsang, Ap-

sornsawan Arwatchanakarn, Wasin Charerntantanakul, Kageeporn Wongpreedee, Nipattra Debavalya, Jumpol Vorasayan, Suphalat Chittamvanich, Napaporn Atichokudomchai, Chontichar Shinatrakool, Vee Shinatrakool, Jumnongjit Phasuk, Prihamdhani Amran, Jian Gong, Ping Xiang, and Haishin Ozawa for their great friendship and support that made my life in Ames wonderful.

Finally, I would give all of my gratitude to my parents, Subhon and Yaowalak Eua-Anant, my sister, Nawanant Piyavhatkul, and my brothers, Navaphol and Nawapak Eua-Anant for their unconditional love, support, and encouragement during my difficult times since I have been far away from home.